Dongil Shin
Department of Mechanical Engineering,
Texas A&M University,
College Station, TX 77840
e-mail: davshin@tamu.edu

Jongin Yang
Department of Mechanical Engineering,
Texas A&M University,
College Station, TX 77840
e-mail: jiyang@tamu.edu

Xiaomeng Tong
Department of Mechanical Engineering,
Texas A&M University,
College Station, TX 77840
e-mail: tongxiaomeng1989@email.tamu.edu

Junho Suh
School of Mechanical Engineering,
Pusan National University,
Busan 46241, South Korea
e-mail: junhosuh@pusan.ac.kr

Alan Palazzolo
Department of Mechanical Engineering,
Texas A&M University,
College Station, TX 77840
e-mail: a-palazzolo@tamu.edu

A Review of Journal Bearing Thermal Effects on Rotordynamic Response

Traditional analysis of journal bearings assumed a constant viscosity which simplified the solutions for static and dynamic characteristics and responses. Today's high-performance machinery requires more accurate models wherein temperature and viscosity distributions in the film must be calculated. Thermal effects in journal bearings have a strong influence on both static and dynamic properties, and consequently play a critical role in determining rotor-bearing system performance. This paper presents an extensive survey of the thermal modeling methods and effects in journal bearings. The subjects include various bearing types, and recent progress in thermal bearing design and thermal instability problems observed in fluid and gas film hydrodynamic bearings. The extent of the survey ranges from conventional Reynolds equation models to more advanced computational fluid dynamics models. [DOI: 10.1115/1.4048167]

Keywords: bearing design and technology, fluid film lubrication, gas (air) bearings, hydrodynamic lubrication, thermoelastohydrodynamic lubrication, viscosity

1 Introduction

Research on thermal effects and their influence on bearing and rotor-bearing performances have gained much attention in the past several decades. Abundant, excellent research has been conducted to accurately predict bearing thermal effects and experimentally verify. This paper summarizes numerous technical papers regarding thermal effects in journal bearings. Thermal effect research has been conducted on various types of bearings, including tilting pad, pressure dam, and flexure pivot journal bearings as reviewed in Sec. 2. Increasing demand for higher speed and power density machinery has led to more frequent observations of thermally induced, bearing related, rotordynamic instability problems. An example is thermal rotor bow instability caused by asymmetric rotor heating in journal bearings, referred to as the "Morton effect (ME)." This topic is treated in Sec. 3. Gas bearing related thermal effect modeling is reviewed in Sec. 4. Computational fluid dynamics (CFD) analysis has gained much attention in bearing thermal effect research as a result of its highly accurate prediction capabilities. A review of journal bearing CFD modeling methods including thermal effects is presented in Sec. 5.

Figure 1 shows a generic tilting pad journal bearing illustrating the pads, pivots, journal, and their corresponding motion coordinates and the film thickness, offset, and preload.

The film thickness equation for the spherical pivot titling pad journal bearing (TPJB) is

$$\begin{aligned} h(\theta, z) = {} & C_P - E_x\cos(\theta) - E_y\sin(\theta) \\ & - (C_P - C_b)\cos(\theta - \theta_P) \\ & - \delta_{tilt}R\sin(\theta - \theta_P) - h_{shaft.TE}(\theta, z) - h_{pad.TE}(h, z) \end{aligned} \quad (1)$$

where

$$E_x = e_x - y_{pvt}\cos\theta_p - z\alpha_{pitch}\cos\theta_p - z\beta_{yaw}\cos(\theta_p + \pi/2) \quad (2)$$

$$E_y = e_y - y_{pvt}\sin\theta_p - z\alpha_{pitch}\sin\theta_p - z\beta_{yaw}\sin(\theta_p + \pi/2) \quad (3)$$

and C_P and C_b are bearing and pad radial clearances, respectively, θ and θ_p are the bearing and pivot circumferential coordinates as shown in Fig. 1(*a*), z and R represent the axial coordinate and the journal radius, respectively, $\delta_{tilting}$, α_{roll}, β_{yaw}, and y_{pivot} represent tilting/rolling/yawing pad angular motions, and pivot deformation, respectively.

The equations of motion for the spherical pivot-type TPJB are shown in Fig. 1(*b*)

$$\begin{aligned} & M_{pad}\,\ddot{y}_{pivot} = -K_P\,y_{pivot} + F_{pad} \\ & I_{tilting}\,\ddot{\delta}_{tilting} = T_{tilting} \\ & I_{roll}\,\ddot{\alpha}_{roll} = T_{roll} \\ & I_{Yaw}\,\ddot{\beta}_{yaw} = T_{yaw} \end{aligned} \quad (4)$$

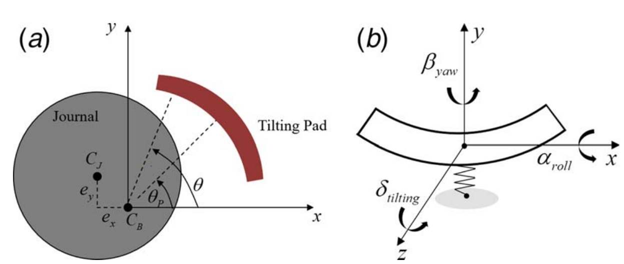

Fig. 1 Tilting pad journal bearing model: (*a*) model for journal dynamics and (*b*) spherical pad pivot type

Contributed by the Tribology Division of ASME for publication in the Journal of Tribology. Manuscript received December 4, 2019; final manuscript received August 12, 2020; published online September 21, 2020. Assoc. Editor: Patrick S. Keogh.

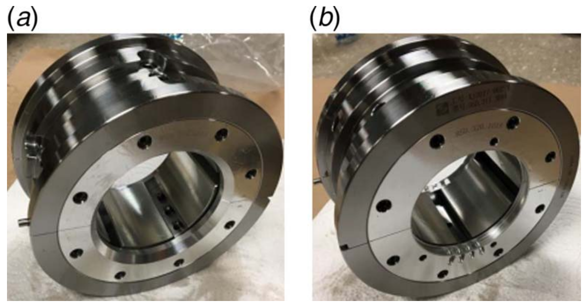

Fig. 2 Photos of tilting pad journal bearing: (a) direct lubrication type and (b) flooded lubrication type

where M_{pad}, $I_{tilting}$, I_{roll}, and I_{Yaw} represent the mass and the rolling/tilting/yawing inertias of pads, respectively, and F_{pad}, T_{tilt}, T_{pitch}, and T_{yaw} are the fluidic force and the inertial moments imposed on a pad, respectively. These bearings are lubricated via direct or flooded lubrication as shown in Fig. 2.

Reference is made throughout the review to the fundamental, governing equations for Reynolds equation-based lubrication analysis including thermal effects. The Reynolds equation is a statement of mass conservation which is expressed in terms of pressure through use of the fluid momentum equations. The viscosity is assumed constant in Reynolds equation for isothermal film models and varies continuously throughout the film for thermohydrodynamic models. This variation is due to the temperature variation which is obtained by solving the (conservation of) energy equation for the lubricant film domain. In turn, the energy equation involves velocities that are obtained from solution of the Reynolds equation. The velocities appear in the dissipation and convective terms in the energy equation as shown below.

Variable viscosity Reynolds equation for lubricant film pressure:

$$\nabla \cdot (D_1 \nabla p) + (\nabla D_2) \cdot \boldsymbol{U}_s + \frac{\partial h}{\partial t} = 0 \tag{5}$$

where

$$D_1 = \int_0^h \int_0^z \frac{\xi}{\mu_f} d\xi dz - \frac{\int_0^h \frac{\xi}{\mu_f} d\xi}{\int_0^h \frac{1}{\mu_f} d\xi} \int_0^h \int_0^z \frac{1}{\mu_f} d\xi dz \tag{6}$$

$$D_2 = \frac{\int_0^{h_f} \int_0^z \frac{1}{\mu_f} d\xi dz}{\int_0^{h_f} \frac{1}{\mu_f} d\xi} \tag{7}$$

Energy equation for lubricant film temperature:

$$\rho_f C_{p,f} \left(\frac{\partial T_f}{\partial t} + U \frac{\partial T_f}{\partial x} + W \frac{\partial T_f}{\partial z} \right) = \lambda_f \left(\frac{\partial^2 T_f}{\partial x^2} + \frac{\partial^2 T_f}{\partial y^2} + \frac{\partial^2 T_f}{\partial z^2} \right) + \mu_f \left[\left(\frac{\partial U}{\partial y} \right)^2 + \left(\frac{\partial W}{\partial y} \right)^2 \right] \tag{8}$$

where h is the film thickness, T_f is the fluid film temperature, U and W indicate the circumferential and axial flow velocities across the film thickness, respectively, U_s is the shaft surface velocity vector, ρ_f is the lubricant density, $C_{p,f}$ is the lubricant specific heat, μ_f is the lubricant viscosity, and λ_f is the fluid film thermal conductivity.

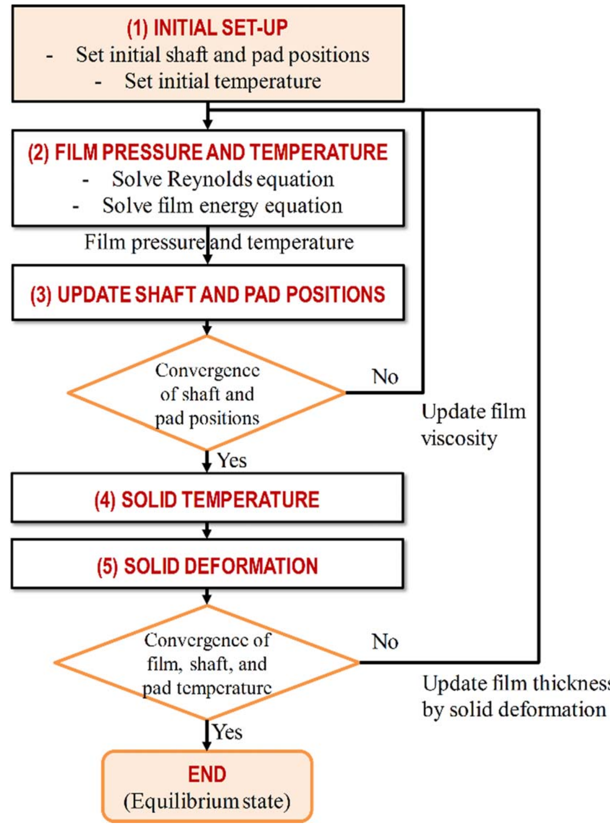

Fig. 3 Generic flow diagram of the thermoelastohydrodynamic (TEHD) journal bearing solution process

Viscosity—temperature relationship:

$$\mu_f = \mu_{ref} e^{-a\,(T_f - T_{ref})} \tag{9}$$

Figure 3 shows a generic flow diagram of the TEHD bearing solution process illustrating the interaction between temperatures, viscosities, pressures, deformations, and equilibrium state iteration.

2 Thermal Effects in Journal Bearings

2.1 Numerical and Experimental Approaches. Knight and Niewiarowski [1] presented a numerical model for the analysis of the thermal behavior of the lubricant in the cavitated region of a journal bearing. A bubbly mixture of liquid and air was assumed. The coupled energy and classical Reynolds equation were solved simultaneously. The predicted data with the assumption of dispersed gas bubbles were compared with published experimental data and an effective length model. Taniguchi et al. [2] presented a three-dimensional thermohydrodynamic (THD) lubrication model of a 19-in. diameter tilting pad journal bearing for a steam turbine with considerations of laminar and turbulent flow regimes. A total heat balance based mixing inlet temperature was calculated to predict the pad inlet temperature. The predicted data including eccentricity, metal surface temperature, and friction loss were compared with experimental data. Knight and Ghadimi [3] presented two different approaches for describing the cavitated zone for THD lubrication analysis that includes the result of pad surface temperature distribution. Their first model assumed a constant ratio between the cavity height and the local gap height, and their second model assumed a constant thickness of the adhered fluid layer. The temperature distribution was evaluated by a first-order energy equation as in the earlier research performed by Knight and Niewiarowski [1]. A heat flux boundary condition between the lubricant and the bearing pad was included. Simmons and

Dixon [4] performed experimental work with a 200 mm diameter, five pad tilting pad journal bearing. The load direction was varied by rotating the bearing in its housing, and it was discovered that the load direction has a critical influence on the maximum pad temperature. Kim et al. [5] presented a finite element (FE), TEHD, two-dimensional tilting pad journal bearing model. The generalized Reynolds equation, with variable viscosity in the axial, circumferential, and cross film directions, and the energy equation were coupled via a temperature-dependent viscosity relation. A Reynolds boundary condition was used by using a modified back-substitution procedure, to impose zero pressure and zero normal pressure gradient at the cavitation boundary. A finite element, up-winding scheme was used to avoid numerical oscillations in the solution of the energy equation. Classic mixing temperature theory (MTT) was used to predict the fluid temperature flowing into the pad. The MTT is expressed by the mixing coefficient formula

$$MC = \frac{(T_o - T_{sup})}{(T_i - T_{sup})} = f\left(\frac{Q_i}{Q_o}\right) \tag{10}$$

where T_i is the temperature of the inlet between pads (BP) (prior pad outlet), T_o is the temperature of the outlet between pads (next pad inlet), and T_{sup} is the oil supply temperature. The mixing coefficient MC is generally applied as a function of Q_i/Q_o(Q_i: inlet flowrate between pads, Q_o: outlet flowrate between pads) depending on Refs. [6–8].

Pad deformations resulted from thermal, pressure and pivot loads, and pivot deflection was based on Hertzian contact theory. Newton–Raphson iteration was applied to determine the equilibrium states including film temperature distribution, pad temperature distribution, pad deformation, shaft temperature, sump temperature, pad tilt angles, and journal position.

Kim et al. [9] presented a TEHD, tilting pad journal bearing numerical model with modal coordinate to reduce the computation time for the analysis of the pad elastic deformation. The full stiffness and damping matrices included modal displacement and velocity coordinates, along with physical coordinates. Their simulation results compared well with earlier experimental work. Gadangi and Palazzolo [10] performed a time transient analysis of tilting pad journal bearing system considering thermal effects and pad deformations. Pad radial deformation was included in the film thickness equation for the evaluation of the fluid film thickness. Three different models were studied: (a) isoviscous rigid, (b) isoviscous flexible pad, and (c) isoadi rigid pad. The thermal effects were found to have little influence on the bearing-journal dynamic behavior, whereas pad deformation had greater effects on the dynamic behavior and the minimum film thickness. Guyan reduction of the two-dimensional (2D) pad elastic FE model was used for computational efficiency, where the pad inner surface degrees-of-freedom were the master degrees of freedom. Desbordes et al. [11] presented a three-dimensional (3D) FE pad model to perform dynamic transient simulations of a journal bearing system considering pad elastic deformation under dynamic loading. Rigid pad tilt motion was used in the transient journal whirling model, and elastic pad deformation was used in the static equilibrium model. This research does not provide any thermal modeling; however, it produces the minimum film thickness and maximum pressure which are closely located with maximum temperature. Fillon et al. [12] studied pad thermal-elastic deformation effects on TPJB dynamic behavior under unbalance loading. A pseudo-time transient analysis was developed for evaluating the effective viscosity of the lubricant and pad thermal-elastic deformation. Both the temperature-viscosity variation and the operating film thickness due to the elastic-thermal pad deformations were found to have a great influence on the dynamic behavior of the bearing. Gadangi et al. [13] investigated bearing thermal effects on bearing-shaft dynamic behavior under a sudden mass unbalance condition. The three different transient analyses were studied: (a) full time transient analysis, (b) linear analysis using dynamic coefficients, and (c) pseudo time transient analysis considering static application of dynamic loads. Monmousseau and Fillon [14] performed a nonlinear transient TEHD analysis for a TPJB under a dynamic loading condition. Both thermal and elastic deformations of bearing pad were considered, and the numerical results compared well with experimental results. Gandjalikhan Nassab and Moayeri [15] presented a computational fluid dynamics (CFD) approach for thermohydrodynamic analysis of an axially grooved journal bearing. The 3D Navier–Stokes equations, coupled with the energy equation, were solved to obtain lubricant pressure and temperatures. Conduction in the shaft, cavitation effects, and liquid fraction in the cavitated region were taken into account. Nicholas [16] concluded that tilting pad bearing operating temperature can be reduced by using (a) evacuated housings with spray bars for directed lubrication, (b) offset pivots up to 65%, (c) spray-bar blockers, (d) babbitted chrome copper pads, and (e) behind-the-pad by-pass cooling.

He et al. [17] developed an adiabatic thermohydrodynamic model for pressure dam bearings, using an effective viscosity to account for turbulence, and an adiabatic energy equation. Fatu et al. [18] presented a TEHD lubrication model for the analysis of dynamically loaded journal bearings. A FE approach was utilized for solving Reynolds equation, and thermal distortions and elastic deformations of the bearing surface were included in the model. Lubricant temperature is regarded as a time-dependent three-dimensional variable. Brito et al. [19] performed an experimental study on the effects of lubricant supply temperature and pressure effects on the performance of a 100 mm plain journal bearing. It was found that a downstream groove had significant effects on the temperature at the oil–bush interface for the high-load and high supply pressure cases. Liu et al. [20] presented a direct solution method of the generalized Reynolds equation, where the pressure and the cavitation zone boundary are determined without iteration and developed a simplified one-dimensional thermal model based on simplifying a two-dimensional model. Their numerical algorithm takes into account the film thermal effects and provides a direct and rapid numerical approach for obtaining the temperature field. Sim and Kim [21] presented a THD numerical approach for flexure pivot, tilting pad gas bearings utilizing the generalized Reynolds equation, 3D energy equation, and heat flux equations. Both rotor thermal and centrifugal expansions were considered. Bang et al. [22] performed an experimental study to compare leading-edge groove (LEG) tilting pad journal bearings with conventional journal bearings under different running conditions. Power loss and pad temperature were measured with and without a toothed seal. Chauhan et al. [23] investigated oil film temperature, load capacity, and power loss for three different oil grades, with elliptical and offset-halves journal bearings. The tested offset-halves journal bearing was found to run cooler compared with a conventional elliptical journal bearing and produced minimum power loss and good load capacity when using a specific oil.

Solghar et al. [24] investigated the influence of the angle between the groove axis and the load direction on the thermohydrodynamic behavior of a twin groove, hydrodynamic journal bearing. The test was performed for different loading directions and provided oil–bush interface temperature, oil outlet temperature, maximum bush temperature, total flowrate, and oil flowrate through each, at constant oil supply temperature. A negative lubricant flowrate was measured at one groove at specific running conditions. Thorat et al. [25] calculated and measured the bearing metal temperatures of a five-pad, load-between-pad tilting pad journal bearing. Temperature was measured at the two loaded bottom pads and predicted by TEHD analysis model. Tschoepe and Childs [26] measured bearing clearance both at room and hot temperatures immediately following tests to obtain the cold and hot clearances. The measured clearances were reduced by 16–25% compared with room temperature clearances. Thermal deformation of the shaft and bearing pads were measured and simulated. Suh and Palazzolo [6,27] presented a tilting pad journal bearing model with TEHD lubrication analysis. Both pad elastic and thermal deformations were taken into account based on a three-dimensional FE model. Modal reduction of the pads was performed, retaining only lower frequency modes for improved computational efficiency. Pivot stiffness was included using Hertzian contact theory. Transient dynamic analysis was performed to determine the static equilibrium condition states by integrating until steady state was reached.

Zhang et al. [28] suggested a corrective structural retrofit of a three-pad tilting pad journal bearing with an 800 mm diameter, used to support an 1150 MW nuclear power generator. In this instance, the bearing experienced in-service local melting damage caused by a local high temperature rise. Kuznetsov and Glavatskih [29] studied the effects of mechanical and thermal deformations of a compliant lining on the dynamic characteristics of a two-axial groove bearing using a THD lubrication model. Compliant lining thickness effects on dynamic coefficients were simulated and compared with conventional babbitted bearings. Li et al. [30] studied journal bearing performance with thermal and cavitation effects for different lubricants, utilizing a transient CFD approach with fluid–structure interaction. The simulation results were compared with published results. Mo et al. [31] performed a transient simulation of journal bearing temperature using the CHD code ANSYS FLUENT. The bearing was used in an internal gear pump, where a complicated shaft motion results from the time varying gear tooth contact load. A test rig was built for comparing test results with simulation. Nichols et al. [32] studied the effects of lubricant supply flowrate on bearing performance at steady state and compared their experimental work with predictions based on a TEHD lubrication model. Bouyer et al. [33] investigated the impact of geometrical defects in two-lobe journal bearing on temperature. Pressure and temperature data were simulated for three scratch depths and compared with experimental results.

2.2 Misalignment Effects. Bouyer and Fillon [34] performed experimental work to investigate the effect of misalignment on the performance of a 100 mm diameter plain journal bearing. Pressures, lubricant temperatures, oil flowrates, and minimum film thickness were measured for various misalignment conditions. El-Butch and Ashour [35] studied the performance of a misaligned tilting pad journal bearing under time varying loading using a TEHD bearing model. Pad elastic and thermal deformations are considered, and a modified film thickness equation is presented to include misalignment effects. Jang and Khonsari [36] studied misaligned journal bearings using a three-dimensional mass-conserving, thermohydrodynamic lubrication model that considers film rupture and reformation. Increased maximum pressure, maximum temperature, bearing load, leakage flowrate, and moment resulted from increasing the misalignment angle, due to decreased minimum film thickness. Sun et al. [37] studied the effect of angular misalignment and surface roughness on pressure, lubricant temperature, load capacity, leakage flowrate, friction coefficient, and misalignment moment. Thermal effects had a large influence on lubricant properties, under the conditions of large eccentricity ratio and misalignment angle. Suh and Choi [38] studied effects of angular misalignment on TPJB performance for different pivot designs. Minimum film thickness, pad thermal deformation, static-dynamic performance, and lubricant peak temperature were simulated versus magnitude and direction of misalignment.

2.3 Numerical Models to Predict Pad Inlet Temperature. Yang et al. [39] performed experimental work to study the impact of lubricant inlet temperature on TPJB performance. Bearing performance characteristics including oil film thickness, temperature rise, and rotor vibration were measured versus inlet temperature. Abdollahi and San Andrés [40] presented a lubricant thermal flow mixing model in a supply groove area to predict an effective bearing pad inlet temperature. Their numerical model considered side leakage flow and utilizes an empirical coefficient. Hagemann and Schwarze [41] performed a finite volume based simulation of the oil flow, mixing, and inlet fluid temperature in a two-lobe hydrodynamic journal bearing. Hagemann et al. [42] studied the heat

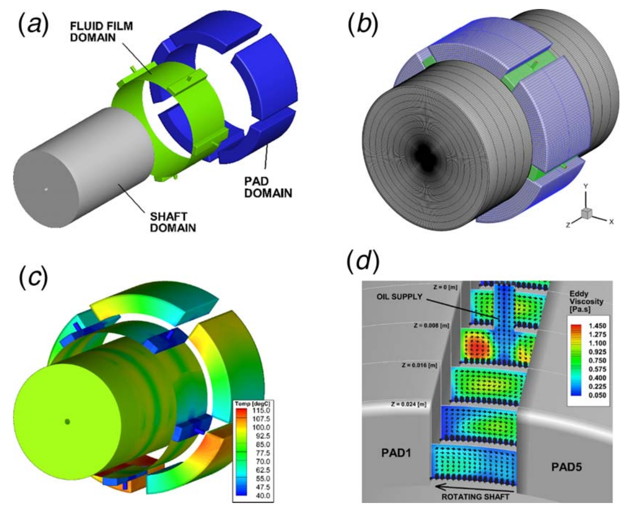

Fig. 4 Geometry, temperature distributions, flows between pads in recent TEHD-CFD TPJB study: (*a*) exploded view, (*b*) overview (420,108 elements), (*c*) temperature distribution, and (*d*) flow between pads [43]

transfer between the leading and trailing pad free surfaces and the space between pad regions using the CFD code ANSYS CFX. The trailing pad free surface heat transfer was found to have a significant effect on the maximum pad metal temperatures. The numerical results were compared with the experimental work performed by the authors. Yang and Palazzolo [43,44] presented a full three-dimensional computation numerical model of TPJB with the consideration of multiphase flow, thermal-fluid, transitional turbulence, and thermal distortion of the journal and bearing pads, adopting two-way fluid–structure interaction. This is represented in Fig. 4. The full 3D CFD model including detailed flow and thermal modeling between pads produced noticeable differences with the classical Reynold's model mixing coefficient approach. Detailed comparisons between the CFD and the Reynolds approach were presented.

3 Thermally Induced Rotor Instability (Morton Effect)

A thermal bearing phenomena which is very challenging to accurately simulate is the so-called "Morton effect." A common use of thermal bearing modeling results is the prediction of the clearance reduction resulting from thermal expansion of the pads and journal. The heat source for this case is the viscous shearing of the lubricant between the journal and the pads. These studies assume that the journal is maintained at a common isothermal temperature, which is certainly the "on average" case if the journal is fixed at its equilibrium position and non-vibrating. However, the assumption of "on average" isothermal journal temperature is not strictly true for the synchronous vibration (whirling) case. A growing number of machines with thermal bow induced, synchronous spiral vibrations led researchers to consider the possibility of non-axisymmetric, journal temperature distributions that would provide the source for the observed dynamic bow. Researchers found that under certain conditions, significant temperature differences (ΔT) can develop across the journal circumference, bending the shaft and leading to potential instability with excessive vibrations. This vibration instability problem that arises from vibration induced asymmetrical journal heating is termed the ME, after the pioneering works of Morton [45] and Hesseborn [46].

Figure 5 illustrates the ME simulation algorithm. The initial conditions for the rotor-bearing state variables are specified in the first step of the algorithm. Then, the transient rotor and TPJB dynamics are calculated by numerical integration until steady-state is reached. This utilizes the dynamic equations with updated film thickness, the Reynolds equation, and the energy equation. Each journal

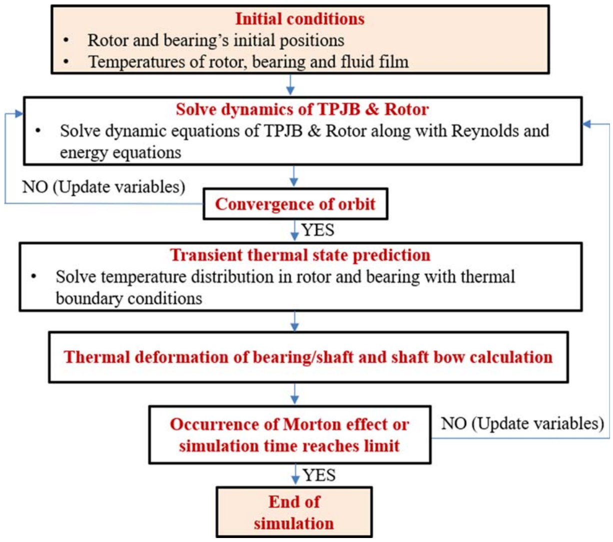

Fig. 5 Nonlinear transient Morton effect prediction flow diagram

orbit is divided into N steps, and the energy equation is solved at each segment to calculate the film temperature and update the variable viscosity. Then, the Reynolds equation coupled with the dynamic equations, are also numerically integrated at each segment with the variable viscosity from the previous step. The algorithm is repeated until the ME instability occurs, or until the specified limit time is reached.

The ME differs from the earlier cases of the "Newkirk effect" [47–50], where the rotor becomes thermally bowed from heat generated by rubbing against the bearings or seals, and displays similar synchronous component spiral vibration with a slowly varying phase angle. The American Petroleum Institute (API) rotordynamics tutorial states "while synchronous thermal instability fits the classic definition of an unstable system, rotor stability codes are currently not used to predict the existence" [51]. This highlights the challenge for designing a rotor-bearing system to avoid the ME. Countering the ME may require significantly dropping the maximum continuous operating speed and therefore the production efficiency. Ignoring the ME may lead to catastrophic damage to the machinery. Researchers have been dedicated to better simulating and preventing the ME. Some excellent case studies and ME theories are reviewed in Refs. [52–54].

3.1 Symptoms. Morton effect frequently occurs in overhung machines including a single-overhung wheel [55], or double-overhung wheels [56], and often with an integral gear [57]. A characteristic symptom of the ME is a spiral vibration in the 1× filtered polar plot at constant rotor rpm, with fluctuating amplitude and changing phase angle [55–58] that usually lasts several minutes for a 360 deg phase change [56,57]. This behavior precludes rotor balancing, which works best with a near constant amplitude and phase angle. The spirals are caused by hot spot's slowly moving around the journal circumference, and the consequent thermal shaft bending (bow), even at constant rotor speed. The rotor bow changes at constant rpm and as an effective imbalance. Therefore, the unbalance response for decreasing speed will differ from its counterpart for increasing speed. This is referred to as the hysteresis like behavior of the ME. The coast-down vibration amplitude is typically much higher than the run up [55,56], which is caused by the rotor temperature recovery lagging the rotor speed due to the rotor thermal inertial.

Perhaps the most vexing characteristic of the ME is a high sensitivity to operating conditions and parameter values. Most reports of the ME in industry describe scenarios where there are multiple "identical machines" and only one experiences the ME. This implies that a small change in some material, geometrical or operating parameter instigates the ME. A slight adjustment of overhung mass/length [59,60], bearing clearance [61,62], bearing L/D ratio [58,62,63], oil temperature [57,64], oil viscosity [56,65], pivot offset [23,25], etc., can mitigate the ME as a consequence of altering the rotordynamics or the viscous shearing inside the bearing. Table 1 lists publications related to bearing change remedies for the ME. In many cases it is more practical for engineers to redesign the bearings rather than the more complicated rotors.

3.2 Experimental Works. Conventional thermal analyses and measurements mainly focus on bearing, not journal, temperatures. However, the ME root cause is the journal circumferential ΔT, and thus acquiring the journal temperature distributions provides an effective benchmark for ME predictions. Generally, the journal temperature is inaccessible in practice and requires special design and instrumentation for the test rig. de Jongh and Morton [59] built a shorter and simplified rotor to replicate the ME in their industrial compressor, which was supported by similar TPJBs. Four resistance temperature detectors (RTDs) were inserted 1.3 mm below the journal surface 90 deg apart and a slip ring-less transmitter was used to transfer the temperature signals from the rotating shaft. They found that the journal ΔT increased significantly from 3 °C at 10.5 krpm to over 10 °C at 11.2 krpm, at which point the rotor speed was forced to decrease to avoid potential damage. They used a total of four equally spaced RTDs to measure the differential temperature on the journal circumference. The phase lag between the high spot and hot spot on the journal was found to be speed dependent. They measured phase lag between the high spot and hot spot was estimated to be 20 deg at 10,500 rpm, and 15 deg at 11,500 rpm.

The complexity of the journal temperature measurement precluded Balbahadur [69] from including these in their test effort. Instead, rotor vibrations were measured during run up, dwelling at a constant speed and during rundown. A hysteresis effect was found where the coast-down vibration amplitude was much higher than the run up from 7500 to 8500 rpm, and the peak vibration coincided with the third critical speed. Panara et al. [70] installed eight thermocouples around the journal circumference, and the temperature signals of the spinning shaft were transmitted to the stator through a wireless slip ring, similar to de Jongh and Morton's experiment [59]. Additional temperature sensors were attached on the bearing pads to compare with predictions. Three overhung weights (12.4%, 8.4%, and 7.3% of the rotor weight) were installed during the test to identify the effect of overhung mass on the ME. Test results showed that the ME instability onset speed decreased with heavier overhung mass and was believed to be related to the shift in rotor critical speed. Tong and Palazzolo [71] measured journal temperature with 20 RTDs equally spaced around the circumference at the mid plane, to benchmark their transient ME algorithm, as shown in Fig. 6.

The shaft was supported by two rigid ball bearings, and the middle rotor stage was intentionally machined to have an offset centerline by 0.003 in., relative to bearing centerline, thus producing a prescribed synchronous journal orbit in the TPJB. Various rotor speed (up to 5500 rpm), static eccentricities (0 and 0.32Cb), and supply oil temperature (28 °C and 41 °C) were tested. The results showed that the journal ΔT increased almost proportionally to the rotor speed, reducing the supply oil temperature reduced the rotor ΔT, and the phase lag between the high and hot spot changed from 20 deg at 1200 rpm to 40 deg at 5500 rpm.

3.3 Morton Effect Prediction. Although still a challenging task, the ability to accurately predict the ME has evolved from early levels characterized by the remark "a not well-known rotordynamic phenomenon" [52]. This progress has resulted from some clever observations of test results and improvements in coupled rotor-bearing thermal modeling. The first theoretical analysis of the ME was proposed by Keogh and Morton [72,73] and utilized

Table 1 Case studies—symptoms and solutions for Morton effect

Cases	Bearing types	Rotor configuration	Symptoms	Solution
de Jongh and Van der Hoeven [55]	Tilting pad bearing	Centrifugal compressor with single overhung wheel	Cyclic synchronous vibration with changing phase at 8500 rpm; hysteresis	Increasing bearing clearance from 0.19% to 0.22%; install heat barrier sleeve
de Jongh and Morton [59]	Tilting pad bearing	Drive-through compressor with double overhung	Hysteresis, large synchronous spiral vibration, sensitive to imbalance	Reduce the overhung weight
Faulkner et al. [66]	Axial groove bearing with pockets in two upper lands	Turbocharger rotor with double-overhung wheels	Cyclic synchronous vibration with changing phase at constant speed over 9800 rpm	Add an undercut in the loaded bearing to increase eccentricity
Berot and Dourlens [58]	5-pad tilting pad bearing	Centrifugal compressor with single overhung wheel	High spiral vibrations at 6510 rpm, quick changes in oil temperature and rotor speed directly trigger instability	Reduce L/D from 0.39 to 0.33
Kirk et al. [62]	5-pad tilting pad bearing	Compressor with a single-overhung wheel	Large synchronous vibration	Increase C_b by 33%, reduce L/D from 0.476 to 0.25
Marscher and Illis [57]	Tilting pad bearing	Integrally geared, two overhung wheels	High cyclic synchronous vibration with 6 min period. Sensitive to supply oil temperature	Increase supply oil temperature from 51.7 °C to 53.3 °C
Schmied et al. [56]	5-pad tilting pad bearing	Turbo expander with double-overhung wheels	Spiral vibrations at 18,600 rpm with period of around 5 min, and hysteresis in vibration	Reduce L/D from 0.6 to 0.4, reduce oil viscosity from 46 cS to 32 cS
Lorenz and Murphy [67]	Partial arc bearing	Single overhung wheel	Spiral synchronous vibrations at 4 krpm; hysteresis vibration; oscillation period of 7.5 min	Replace the partial arc bearing with four-lobe fixed pad bearing
Childs and Saha [65]	Plain journal bearing	Symmetric rotor with double-overhung disks	High synchronous vibration	Reduce lubricant viscosity, increase L/D ratio
Suh and Palazzolo [68]	Tilting pad bearing	Single overhung rotor	Spiral vibration and hysteresis	Reduce supply oil temperature, increase C_b
Tong and Palazzolo [64]	Tilting pad bearing	Double-overhung rotor	Spiral vibration and hysteresis	Increase pivot offset, use direct lubrication, increase oil temperature

short bearing theory, the laminar flow energy equation, and a heat conduction model of the bearing and journal. The rotor thermal bending was calculated from the asymmetric heating and incorporated into the rotordynamics model. Classical feedback theory was implemented to determine instability conditions over the design speed range. Larsson [74,75] extended Keogh and Morton's theoretical model and applied it for the ME instability analysis of a rotor system with five-pad TPJBs. Parametric studies of the bearing thermal model including the air-convection coefficient and the bearing width. Tucker and Keogh [76] applied CFD to analyze the pressure and thermal states in a hydrodynamic journal bearing with a whirling shaft over its prescribed orbit. The Navier–Stokes equations and the energy equation were solved simultaneously for both the lubricant flow velocity and temperature. The heat flux and temperature were set to be continuous on the film/bearing and journal/film surfaces, and the rotor surfaces beyond the bearing width were imposed with heat convection conditions. For a centered circular orbit, significant journal ΔT, as high as 7 °C, developed with an orbit size of $0.58C_b$. Gomiciaga and Keogh [77] extended Tucker's method to investigate the non-centered orbit case based on a two-inlet circular bearing. The asymmetric heat into the journal was obtained by orbit time averaging, and the steady-state journal ΔT was found to (1) increase with speed, however, level off at high speed due to the reduced lubricant viscosity and (2) increase linearly with the journal orbit ϵ when $\epsilon < 0.2C_b$. In 2003, Kirk and Balbahadur [62,63] adopted an unbalance threshold approach for ME prediction. An initial mechanical imbalance U_0 with specified magnitude was set at the overhung location. The journal circumferential temperature could be acquired by solving the one-dimensional simplified energy equation, which neglected time dependence and axial heat flow, and then the resultant imbalance was calculated by vector summing the initial mechanical imbalance and the thermal imbalance

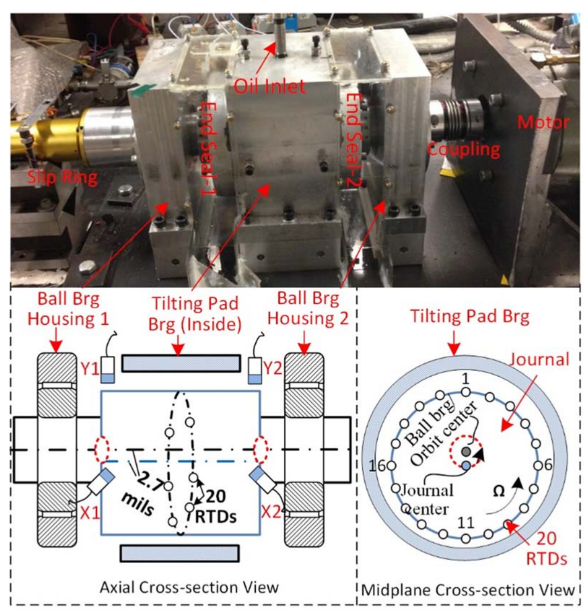

Fig. 6 Photos of test rig and the sensor locations on the journal [71]

from the rotor thermal bending. If the resultant magnitude exceeded the defined threshold, i.e., $1.5U_0$, the rotor was diagnosed as "unstable." Schmied et al. [56] introduced the thermal ratio method to determine ME instability in 2005. The rotor is considered susceptible to

ME if the ratio of the added to eliminated heat was close to a threshold level or above that level. In the reference, the maximum and minimum threshold level of the ME instability is defined by assuming 50% and 100% of added heat, respectively. If the heat ratio of the rotor is within the threshold range, the rotor is determined to be susceptible to the ME.

The thermal ratio curve could be made to shift downward and mitigate the ME by reducing the heat input in the bearing, such as reducing the lubricant viscosity. In 2011, Murphy and Lorenz [78] proposed an intuitive-analytical ME prediction approach, utilizing three linear coefficients $\bar{A}$, $\bar{B}$, and $\bar{C}$ to characterize the relationship between the imbalance, vibration, and journal ΔT, as shown in Fig. 7.

The combination of three serial subfunctions $\bar{B}\bar{A}\bar{C}$ was equivalent to an overall feedback gain $G(s)$. The journal orbit is divided into 24 segments, and the steady film temperature profile was calculated at these 24 points and averaged to obtain an approximate, averaged journal surface temperature profile. A double-overhung turboexpander [56] was provided as a verification case and the predicted ME onset speed was close to the observed speed. In 2012, Childs and Sara [65] calculated the journal temperature by adding the rotor temperature component from the forward and backward orbits. In 2012, Lee and Palazzolo [79] proposed a THD tilting pad, journal bearing ME model with variable viscosity obtained by solving the 2D energy equation for film temperature. An insulated thermal boundary condition was imposed at the fluid/bearing surface, and no pad thermal conduction was included. To reduce the computation cost, a staggered scheme was proposed to perform the transient analysis of the rotor/bearing dynamics as well as temperature. Suh and Palazzolo [6,27] extended Lee's approach in 2014, by adopting a high-fidelity TEHD bearing model to solve for the axial, radial and circumferential lubricant temperature with a 3D energy equation. In 2015, Grigor'ev et al. [80] applied a perturbation method to solve for the oil pressure and temperature and adopted an averaging method to solve for the rotor and bearing dynamics. Tong et al. [81] adopted a more accurate bowed-rotor dynamics model, replacing the approximate equivalent, thermal imbalance model. A more general rotor model with double-overhung disks and multi-bearing capability was developed for transient analysis [82]. In 2018, Tong and Palazzolo [83] extended the transient, high-fidelity ME methodology to a gas TPJB system with 3D FEM and found that the ME could also occur in tilting pad gas bearings and may be sensitive to the mechanical imbalance and overhung mass.

3.4 Challenges. The first challenge for effective ME prediction is setting up a high-fidelity thermal model for the coupled bearing-rotor-film system. Accurate TEHD analysis is a prerequisite for accurate ME prediction, and realistic thermal boundary conditions must be included. Khonsari and Beaman [84] reported that changing the pad thermal boundary conditions would affect the rotor temperature, and adiabatic conditions would overpredict the shaft temperature by 2 °C. In classic TEHD analysis, the detailed shaft temperature distribution is not a significant concern and is usually assumed to be isothermal and calculated by either averaging the oil temperature [85] or imposing the no net-heat flow boundaries conditions on the shaft-film surfaces [84,86,87]. These assumptions are not applied in ME analysis, and special care must be taken to impose proper thermal boundary conditions on the rotor. Lee and Palazzolo [79] conducted the transient ME analysis by neglecting

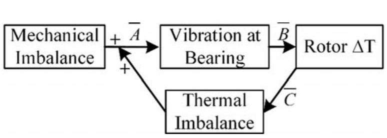

Fig. 7 Linear coefficients illustrating the relationship between the imbalance, vibration, and journal ΔT

the axial temperature variation of the shaft and imposing insulated boundary conditions on the film/bearing surface. The predicted rotor ΔT was found to be higher than Gomiciaga and Keogh's CFD results [77], where a more realistic boundary conditions were imposed based on the temperature and flux continuity on the rotor/film, film/bearing surfaces, and heat convection on external solid surfaces. Similar boundary conditions were imposed by Tucker and Keogh [76]. Both Tucker and Keogh [76] and Gomiciaga and Keogh [77] took account of the circumferential and axial vibration of the journal temperature, thus offering a more accurate prediction of the rotor ΔT. The rotor circumferential ΔT was found to decay fast beyond the bearing length, indicating that rotor sections away from the bearing would not contribute to the thermal bow. Thus, Suh and Palazzolo [68,88] and Tong et al. [82,83] only solved for the detailed temperature distribution of the thermal rotor, i.e., the rotor section close to the bearing location, which experienced temperature rise. Seven times the bearing length was selected as the thermal rotor length to balance the computation cost and accuracy.

The second challenge for effective ME prediction is accurate prediction of the phase lag between the high spot and hot spot on the journal. The high spot and hot spot indicate the journal circumferential location with the minimum thickness and the highest temperature, respectively. The hot spot usually lags the high spot, and accurate prediction of the hot spot relative to the high spot is very important, especially in the simplified analysis, where the thermal imbalance is assumed to be exactly out of phase with the hot spot. To simplify the journal temperature model, a constant phase lag between the hot spot and high spot are usually assumed, for instance, Kirk and Guo [63] assumed that the hot spot coincided with the high spot, and Murphy and Lorenz [78] adopted a constant 20 deg angle. This assumption, however, was proven to have limited reliability and may lead to unsuccessful prediction of the ME instability. de Jong and Morton [59] experimentally found that the phase lag was speed dependent, varying from 20 deg to 15 deg when the speed decreased from 10 rpm to 4 krpm. Tong and Palazzolo [71] found that the hot spot lagged the high spot by 20 deg at 1200 rpm and this angle increased to 40 deg at 5500 rpm.

4 Thermal Effects in Gas Journal Bearings

The literature on the thermal effects in gas bearings has mainly focused on bump foil bearing applications. A representative drawing of a bump foil bearing is shown in Fig. 8. Most of this extensive work has been conducted over the last two decades.

4.1 Energy Equation for Compressible Fluid. The 3D energy equation for the gas bearing is

$$\rho c_p\left(\frac{\partial T}{\partial t}+u\frac{\partial T}{\partial x}+w\frac{\partial T}{\partial z}\right)=k\left(\frac{\partial^2 T}{\partial x^2}+\frac{\partial^2 T}{\partial y^2}+\frac{\partial^2 T}{\partial z^2}\right)+\left(u\frac{\partial P}{\partial x}+w\frac{\partial P}{\partial z}\right)+\Phi \quad (11)$$

where $\Phi=\mu[(\partial u/\partial y)^2+(\partial w/\partial y)^2]$ and ρ is the gas density, c_p is the gas specific heat, u, w are the velocity components in the circumferential/axial directions, and μ is the viscosity. The velocity field u and w are acquired from the pressure gradient predicted by the Reynolds equation. Note that μ is temperature-dependent viscosity which should be updated as the film temperature is updated from the energy equation. The thermo-viscosity relationship is typically modeled with a linear function as $\mu(T)=\mu_0+\alpha T$, where T is temperature. Salehi and Heshmat [90] and Salehi et al. [91] used a simplified energy equation based on a Couette approximation to predict the gas film temperature in the bump foil bearing. The simplified expression was solved with a finite difference technique along with iteration procedures.

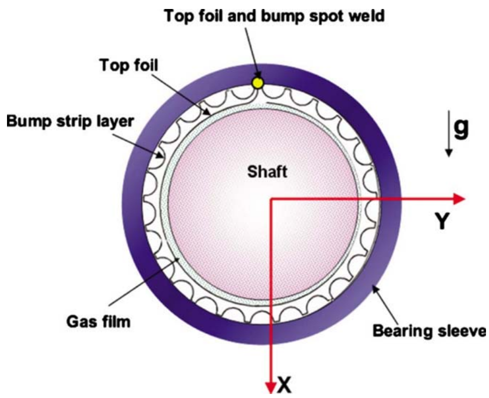

Fig. 8 Schematic of bump foil bearing [89]

A comparison of the predicted temperature with experimental results showed good agreement revealing that the presented numerical approach suggests reasonable estimation of the gas film temperature. Kim and San Andrés [92] developed the bump foil bearing system with 2D bulk flow equation, 2D FE top foil structural model and lumped parameter thermal models of the top foil, bump foil, cooling channel, bearing housing, and shaft. Thermal expansion of the bearing pad and shaft centrifugal growth due to high operating speeds were also taken into account in the model. The prediction from the model showed good agreement with test results. Peng and Khonsari [93] developed a THD model for a bump foil bearing using the 3D energy equation. The cooling effect was considered in the analysis by approximating the forced convection coefficient using Nusselt numbers. The accuracy of the model was verified via temperature prediction comparison with the experiment. The effect of cooling flow was investigated and revealed that the temperature rise of the film increased exponentially with operating speed.

4.2 Modeling of the Detailed Thermal Structures. Lee and Kim [94] used more advanced heat transfer models of the bump foil bearing's substructures including the top foil, bump foils, bearing sleeve, and shaft. The hydrodynamic force and air film temperature was predicted with a generalized Reynolds equation and 3D energy equation. The measured heat transfer resistance between the bearing and top foil is implemented into the model for better accuracy. Parametric results showed the importance of thermal management to avoid the thermal runaway problem. Sim and Kim [95] improved the THD model of bump foil bearing by taking into account the bump thermal contact and inlet flow mixing phenomena. The thermal contact resistance of bump contacts is analytically derived, and the mixing ratio of the inlet flow is determined with CFD analysis. The comparison with experimental results showed that more accurate prediction is achieved with the thermal contact model. A novel cooling method is also introduced which shows effective cooling effect.

Gita and Carpino [96] included the membrane and bending strains of the top foil due to the thermal effect. The bulk flow model for gas film temperature prediction and simple thermal models of the bearing housing, shaft and foils are included. The foil deflection is estimated by assuming the top foil temperature varies linearly. From the analysis, it is verified that the film thickness of the bearing side edge can be overpredicted without considering the deflection in the foils. Lehn et al. [97] suggested an analytical formula for the effective thermal resistance of foils. The formula takes into account the bump geometry, surface roughness of top, and bump foils. They found that the thermal resistance between top and bump foils is independent of the applied load, indicating the injection of cooling flow is necessary to prevent the thermal runaway problem in the foil bearing.

4.3 Computational Fluid Dynamics Analysis. Paouris et al. [98] used CFD analysis to simulate the coupling of compressible fluids and structures. They determined that the incompressible non-THD and compressible THD theories show good agreement in the prediction of load-carrying capacity if the global bearing compressibility is low. The compressible/incompressible Reynolds equation and foil deformation are iteratively solved until global convergence is achieved. A simple finite element method (FEM) is also used to model the bump foil-cooling channel to predict the heat flux from the top foil to a bump foil channel. Aksoy and Aksit [99] developed the coupled TEHD model using a commercial FEM code and a 2D bulk flow equation for the gas film temperature prediction. They verified that the higher gas film temperature is generated with increasing shaft speed. The external cooling flow is essential in the bump foil bearing to avoid the thermal instability including bearing seizure.

4.4 Different Bearing Applications. The thermal effect in non-bump foil gas bearings has also been investigated. Sim and Kim [21] developed a compliant flexure pivot tilting pad gas bearing based on a 3D energy equation and heat flux equations imposed on the interface between the bearing and its surroundings. The parametric studies revealed that the bearing radial clearance affected the temperature distribution significantly. A comparison between the adiabatic and cooling boundary conditions on the bearing was performed, and an abrupt rise in the temperature with the adiabatic conditions was observed. Thermal effects in bump foil thrust bearings (BFTB) was investigated by many researchers. Lee and Kim [100] considered 3D thermal effect on novel designs of BFTB. The bearing types had radially arranged bump foils and preformed step contours on the top foil. Parabolic distribution with operating speed was found on the thrust disc temperature distribution. Abrupt increases in the temperature were attributed to the thermal expansions of the thrust disc and plate. Gad and Kaneko [101] conducted a THD analysis of the BFTB with a 2D energy equation and a simplified energy equation using a Couette approximation. Various configurations of the bump foil were designed to modify the bearing stiffness by changing the direction of the bump foil clamp, height of the bump pitch, and adding bump stiffeners and increasing the number of bump foils. It was found that the different designs affect the bearing performances such as the load-carrying capacity, friction loss, bump foil compliance, etc. Lehn et al. [102] presented a 3D TEHD analysis for a BFTB. The thermal expansion model of the rotor disk was taken into account using the axisymmetric Navier–Lame equations, and the effective thermal resistance of the bump foils was incorporated. The thermal runaway phenomena which shows decreasing load-carrying capacity above a certain critical speed was investigated, and the root cause of this effect was found to be the thermally induced bending of the rotor disk.

Qin et al. [103] modeled the coupled fluid-structure-thermal model of a BFTB using CFD. Both air and CO_2 were used for the working fluid with the same geometry, and the results were compared. It was found that CO_2 generates more power loss and heat than the air for the same operating condition but shows an improved cooling efficiency. The centrifugal pumping only observed in CO_2 helps transfer the dissipated heat to the fluid, which allows effective cooling in the CO_2 bearing. Feng et al. [104] conducted a THD analysis of a spherical spiral groove gas bearing. The numerical results showed that the gas temperature and pressure fluctuate near the spiral groove region due to its discontinuation in the film thickness. Higher load capacity was observed in the THD analysis compared with the isothermal case, and the discrepancy decreased when the thermal expansion was considered in the THD analysis. It was also revealed that the depth of the grooves influences the gas pressure and the suck flowrate in the bearing. Zhang et al. [105] developed a numerical model of a hybrid bump-metal foil bearing which incorporates the metal mesh blocks in its substructures. Detailed thermal models of bump foil, top foil and metal blocks were constructed, and the test was performed to validate the static and dynamic prediction of the model. Various cooling conditions using air flow in the hollow shaft were tested to avoid an excessive temperature in the bearing.

Feng and Kaneko [106] performed a THD analysis of multi wound foil bearings utilizing the Lobatto point quadrature, which consider the lubricant as a compressible gas with variable viscosity. From the analysis, it was found that the highest air film temperature occurs near minimum film thickness and is closer to the top foil than the shaft surface. Higher load capacity was predicted with the thermal model, and the operating speed was the main influence on the temperature rise in the bearing. THD analyses with CO_2 fluid as a lubricant have been conducted. Kim [107] analyzed a foil bearing for a Brayton cycle with supercritical CO_2. To consider the inertia effect in the CO_2 film, a modified Reynolds equation was solved with iterative process, which is coupled with 3D energy equation. The thermal and transport properties of the CO_2 was obtained from the data in REFPROP. The developed model under predicts the power loss when it is compared with the test data, but the difference decreases with higher operating speed. Chien et al. [108] developed a journal bearing lubricated with SCO_2. They used a dynamic viscosity model which is dependent on both pressure and temperature of a lubricant. Different boundary conditions on the bearing were tested to see its effect, and they resulted in different bearing performances.

4.5 Thermal Instability Problems. The high operating speed of bump foil bearings can instigate a thermal instability if appropriate cooling is not provided. Lee et al. [109] developed a transient 3D THD model of a three-pad foil bearing and verified its accuracy by comparing with experimental results. They found that a small amount of cooling air can suppress an unexpected bearing temperature increase. Samanta and Khonsari [110] analyzed a thermoelastic instability problem in bump foil bearings. They derived an analytical closed-from solution to predict the critical speed where a thermoelastic instability occurs in bump foils. It was verified that the wave number and film thickness influence the instability critical speed significantly. Tong and Palazzolo [83] investigated the instability caused by a thermal bow effect (Morton effect) in a rotor supported by tilting pad gas bearings. Using transient and highly fidelity 3D thermal models of film, rotor and bearing, they verified that the Morton effect can occur in the gas bearing as well as an incompressible fluid film bearing.

4.6 Experimental Work

4.6.1 Temperature Measurement. DellaCorte [111] developed a foil air bearing test rig which operated up to 70,000 rpm and 700 °C temperature. The test rig was equipped with a monitoring system to measure the bearing load capacity, torque, speed, and temperatures. DellaCorte et al. [112] tested a foil bearing operating with a journal surface with PS304 coating. The measurement result verified that the coating and bearing design provides improved wear lives for long term operations and good performances over various load conditions. Radil and Zeszotek [113] measured temperature profiles of a foil bearing operating at operating speeds from 20 to 50 krpm and loads from 9 to 222 N. Temperatures and thermal gradients in the axial and circumferential directions of the bearing were measured using thermocouples installed at the backside of the bumps. They found that the maximum temperature occurs at the edge of the bearing while the minimum film thickness was observed at the bearing center. High thermal gradients were observed in the bearing axial direction, and the thermal gradient in the circumferential direction was negligible.

Zywica et al. [114] carried out an experiment with a foil bearing coated with synthetic materials. Four thermocouples were initially installed at the top foil to measure the temperature, but they were damaged due to the wear between journal and the bearing. They introduced a new temperature measurement method using thermovision which turned out to be effective in measuring the temperature. Abraham Chirathadam and San Andres [115] measured the rotordynamic response and temperatures of a metal mesh foil bearing. A heater was installed at the inner surface of a hollow shaft to see the temperature effect on the rotor response. The measured data showed that with sufficient cooling air flow, the temperature input from the heater does not significantly affect the rotordynamic performances.

4.6.2 Softening Stiffness Due to Temperature. A unique feature of a bump foil bearing is the bump foil stiffness variation with bearing temperature. Howard et al. [116,117] measured the dynamic stiffness damping values of a foil bearing, while the temperature was varied from 25 to 538 °C. Significant decrease in the stiffness magnitude up to a factor of two had been observed from 25 to 538. Also it was observed that the damping characteristics of the bearing changes from a viscous type to a friction damping with higher temperature conditions. Kim et al. [118] analyzed the static load and dynamic force characteristics of a foil bearing with increasing temperatures. The heater was installed in the fixed hollow shaft and the heater temperatures varied from 22 to 188 °C. Static and dynamic single frequency loads were applied to measure the bearing load capacity, stiffness, and viscous damping in the test rig. It was also observed that the structural stiffness of the bearing decreases by a factor of three when the shaft temperature was increased to 188 °C. San Andrés et al. [89] measured the stiffness and viscous damping coefficients of a foil bearing with a variable heater temperature applied to the inner side of a hollow shaft. Increases in the coefficients were found with high temperature, which was caused by an increased preload due to the temperature increase.

4.6.3 Thermal Runaway and Its Prevention. Reports of foil air bearing thermal runaway appear in the literature. Thermal runway occurs when excessive thermal expansion and elastic deformation cause reduced film thickness, resulting in bearifng seizure. Dykas and Howard [119] reported a failure on a rotor supported by a foil bearing at NASA Glenn Research Center. The incident occurred at high operating speeds, resulting in a melted region on the top foil. The root cause of the failure was found to be the non-uniform heating of the shaft, leading to the incensed viscous heating which resulted in the bearing seizure. Ryu and San Andrés [120] observed a thermal runaway failure caused by nonuniform heating. The heater was installed at the inner surface of the hollow shaft. The test rig without cooling air flow exhibited violent vibration with the heater temperature at 600 °C and resulted in the melting of the top foil.

Żywica et al. [121] observed a thermal runaway failure in a test rig powered by an electro-spindle shaft with maximum operating speed of 24,000 rpm. At 15,000 rpm, the test rig encountered an unexpected rapid temperature increase in the top foil reaching up to 130 °C and the shaft for 200 °C. The damage on the top foil indicated the decreased air film thickness between the shaft and top foil. Many thermal management techniques for foil bearings were tested experimentally to cure this thermal runaway failure. The bump foil stiffness diminishes with temperature rise, which will reduce the load-carrying capacity. Radil et al. [122] stressed the importance of foil bearing radial clearance design to prevent thermal runaway failure. In their test rig, the optimum value of radial clearance ensured the maximum load capacity coefficient. With a radial clearance smaller than the optimum value, it was found that the rotor was prone to thermal runaway failure. However, foil bearing with clearance values above the optimum were relatively free from failure. Radil et al. [123] tested three different thermal management techniques to avoid the thermally induced problems in a foil bearing. The first method which blows air directly on the journal's inner surface turned out be effective in decreasing the bulk temperature and thermal gradient uniformly. The second scheme blew air inside the journal parallel to the shaft axis, which is a more indirect method than the first, and this method also worked on the reducing the bulk temperature but not as effective as other methods. The third technique was to extract heat from the journal by injecting air axially via the bearing support, which was also effective in cooling the bearing. Radil and DellaCorte [124] developed a three-dimensional power loss map with respect to the load and operating speed for a foil bearing. The map can be separated into low- and high-load regions. The high-load region lies in the left side of the curve's minimum point, and the bearing is prone to the thermal runaway failure in this region. The low-load region, which is the right side of the minimum point shows more stable response but may suffer from an excessive axial thermal gradient, resulting in failure.

Ryu and San Andrés [125] performed a test with a foil bearing and hollow shaft which was warmed by a heater. They verified the cooling effect which is applied by forcing air at the rotor mid span during the foil bearing testing, and results showed that the cooling effect had little effect on the rotor vibration response and is prominent when the rotor is hottest. A computational model was developed and showed good agreement with the test data. Sim et al. [126] conducted an experiment with cooling air flow applied tangentially into the mixing zone of a foil bearing. The thermal management scheme was found to be effective in cooling the bearing, which was evidenced by the increased radial clearance and decreased thermal expansion of the shaft.

5 Computational Fluid Dynamics Thermal-Fluid Bearing Modeling

5.1 Overview of Computational Fluid Dynamics Modeling Studies. The Reynolds equation approach has been widely utilized to model thin film, liquid, and gas bearings. This has limitations that include complex 3D inertia-dominant flow, thermal flow, turbulence, cavitation, and over-simplified physics in supply oil grooves. In particular, the over-simplified physics in the supply oil groove can result in significant errors in the performance prediction of the bearing [43,44,127–131]. CFD modeling can overcome the limitations of the Reynolds approach. The CFD approach utilizes the full Navier–Stokes equation for modeling the bearing flow and temperature. Adopting the incompressible Reynolds-averaged Navier–Stokes (RANS) method [43] for turbulence modeling, the governing equations of the continuity, momentum, and energy can be written as follows.

Governing equations of the CFD approach:

$$\frac{\partial \rho_f}{\partial t} + \frac{\partial}{\partial x_i}(\rho_f u_i) = 0 \tag{12}$$

$$\frac{\partial \rho_f u_i}{\partial t} + \frac{\partial}{\partial x_j}(\rho_f u_i u_j) = -\frac{\partial p'}{\partial x_i} + \frac{\partial}{\partial x_j}\left[\mu_{eff}\left(\frac{\partial u_i}{\partial x_j} + \frac{\partial u_j}{\partial x_i}\right)\right] + S_M \tag{13}$$

$$\frac{\partial \rho_f h_{tot}}{\partial t} - \frac{\partial p}{\partial t} + \frac{\partial}{\partial x_j}(\rho_f u_j h_{tot}) = \frac{\partial}{\partial x_j}\left(\lambda_f \frac{\partial T_f}{\partial x_j} + \frac{\mu_t}{\mathrm{Pr}_t}\frac{\partial h_f}{\partial x_j}\right) + \frac{\partial}{\partial x_j}[u_i(\tau_{ij} - \rho_f \overline{u_i u_j})] + S_E \tag{14}$$

$$\frac{\partial \rho_f}{\partial t} + \frac{\partial}{\partial x_i}(\rho_f u_i) = 0 \tag{15}$$

$$\frac{\partial \rho_f u_i}{\partial t} + \frac{\partial}{\partial x_j}(\rho_f u_i u_j) = -\frac{\partial p'}{\partial x_i} + \frac{\partial}{\partial x_j}\left[\mu_{eff}\left(\frac{\partial u_i}{\partial x_j} + \frac{\partial u_j}{\partial x_i}\right)\right] \tag{16}$$

$$\frac{\partial \rho_f h_{tot}}{\partial t} - \frac{\partial p}{\partial t} + \frac{\partial}{\partial x_j}(\rho_f u_j h_{tot}) = \frac{\partial}{\partial x_j}\left(\lambda_f \frac{\partial T_f}{\partial x_j} + \frac{\mu_t}{\mathrm{Pr}_t}\frac{\partial h_f}{\partial x_j}\right) + \frac{\partial}{\partial x_j}[u_i(\tau_{ij} - \rho_f \overline{u_i u_j})] \tag{17}$$

where h_{tot} and h_f are the total and fluid enthalpy, τ is the stress tensor, and the μ_{eff} is effective viscosity. The μ_t and Pr_t terms are the turbulent viscosity and Prandtl number, respectively, and p' an p are the modified and static pressures.

The inertia-less form of the Reynolds equation can be derived after combining the continuity and momentum equations and neglecting inertia effects. The Reynolds and energy governing equations are given in Eqs. (5) and (8), respectively. By comparison between the full RANS and Reynolds equation, it is clear that the inertia effect is neglected in the form of the Reynolds equation in Eq. (5). A significant drawback of the Reynolds approach is the uncertainty of the fluid temperature within the bearing's non-pad regions that provide pad inlet temperatures. Most common Reynolds models use very approximate treatments of the physical phenomena in grooves or BP as seen in Fig. 9. The inlet temperature is estimated from a simple heat balance with a complete mixing assumption utilizing assumed mixing coefficients (MC). The mathematical relation for the pad inlet temperature (T_{out}) of the fluid film can be expressed as Eq. (10).

The MC is an assumed parameter, generally lacking a physics-based evaluation, and typically ranges from 0.4 to 1. Care should be exercised in interpreting reported MC since its definition varies somewhat in the literature [6–8,132]. The utility (and weakness) of the Reynolds model's MC is it does not require detailed information of the thermal flow between pads. In contrast, the CFD approach predicts sophisticated physical phenomena in the grooves, including three-dimensional transitional turbulence, thermal fluid, and cavitational flow. This advantage of the CFD can provide better accuracy of the journal bearing performance prediction.

The Reynolds modeling approach has evolved over the last half-century, to include 3D turbulence, cavitation, thermal modeling of the fluid film, shaft, and pads, thermal-elastic deformation of the shaft and pads, pad flexibility, pivot flexibility, and development of mixing theory. CFD based bearing modeling [42–44,76,127–131,133–146] has become more commonplace in the literature mainly as a result of the development of low cost, high-performance computers [135,136]. This work focused on the development of high-fidelity modeling techniques, or including effects such as turbulence, thermal flow, and cavitation. CFD has been utilized to improve bearing performance by improving the accuracy of related predictions, especially for varied types of lubricants, multiphase flows, flows with significant inertia effect, and cavitation [129,147–153]. CFD techniques have been applied to textured bearing modeling [154–159] which are bearings designed to reduce drag torques and power loss.

Computational fluid dynamics based bearing studies were mainly performed utilizing commercial CFD software such as CFX [43,44,127,129,130,137–141,152], FLUENT [131,135,142,148–151,153,157], ADINA [143,158], OPENFOAM [128,144], and others [134,136,145,155]. A few studies [76,133,147] utilized inhouse-based CFD codes.

5.2 Computational Fluid Dynamics Modeling: Plain Journal Bearing. Most CFD based bearing research for

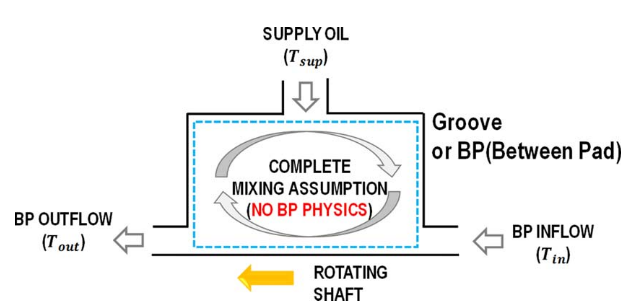

Fig. 9 BP (groove) thermal flow in Reynolds approach

performance prediction has focused on modeling the plain journal bearing [76,127,128,133–137,143,144,146], and first appeared during the period 2010–2015. Tucker and Keogh [133] utilized CFD for modeling a plain journal bearing, considering the full 3D fluid film, shaft, and bearing for solving the fluid flow and energy equations. Thermal aspects of single-inlet and two-inlet groove cases were investigated, utilizing a simplified groove geometry. The results showed the existence of significant radial temperature variation in the fluid film and groove regions. These author's publication [76] considered the case of a centrally located synchronous, forward, circular whirl orbit and showed notable journal temperature differentials in the circumferential direction. This is quite different than the non-whirling case where the journal is on average isothermal. The predicted results were compared with experimental measurements.

Guo et al. [127] conducted CFD thermal fluid modeling of hydrodynamic and hydrostatic journal bearings, focusing on the fluid film and realistic inlet grooves. The study showed that the CFD approach computational time greatly exceeded that for a Reynolds equation-based solution. The results showed good agreement between CFD and Reynolds for static results and stiffness coefficients, but the CFD damping values were larger than their Reynolds counterparts. The reason for this difference was stated as the influence of the fluid in the inlet pockets, as considered only in the CFD model.

Shenoy et al. [134] presented an elasto-hydrodynamic bearing model using fluid structure interaction (FSI) techniques, by coupling the CFD and structural models. The thermal effect was not considered. Maneshian and Gandjalikhan Nassab [146] investigated THD bearing responses under a fully turbulent flow regime, with high Reynolds number. They adopted the AKN low-Re *k*-epsilon turbulence model and proved its validity by the comparison with experimental work. The groove modeling was simplified by prescribing periodic boundary conditions. Liu et al. [143] presented CFD-based FSI modeling including the elastic deformation of the plain journal bearing. The researchers considered a dynamic rotor-bearing system with 3D isothermal fluid film, shaft, and bearing. The elastic bearing deformation showed a significant effect on the rotordynamics. The oil groove and thermal effect were not considered.

Guo et al. [127] developed a 3D CFD model for a journal bearing in steam and heavy-duty gas turbine service. The experimentally verified model included 3D multiphase and thermal flow for the cavitation (air entrainment) in the fluid film domain. The model assumed constant shaft temperature and thermally insulated bearings. The cavitation model was based on the Rayleigh–Plesset theory, and they used the realizable *k*-epsilon model by careful consideration of the turbulence in such a large-scale bearing. The results showed that CFD could enable a detailed examination of the thermal mixing phenomena in the groove region.

Li et al. [135] presented a CFD-FSI model including a flexible rotor and a two-inlet groove journal bearing. The dynamic mesh method in FLUENT was used to achieve optimal grid quality during the transient simulation. The model was utilized for investigating journal misalignment, which had a significant effect on bearing pressure distribution and friction torque but did not significantly impact fluid film force and attitude angle.

Lin et al. [136] extended the CFD model of Li et al. [135] by including thermal fluid and thermal deformation effects. Comparison with experimental work validated the theoretical model. Their results indicated that film temperature increases with speed (rpm), and the film temperature, cavitation volume fraction, and eccentricity ratio decreased with increasing the number of inlet grooves. Thus, the researchers stressed that multiple grooves could have a positive effect on bearing performance.

Song and Gu [137] utilized a 3D thermal-fluid model for simulating a two-axial groove journal bearing, neglecting thermal-elastic deformation effects. The researchers emphasized the importance of the air entrainment and used a gaseous cavitation model. Three phase-change models: Half-Sommerfeld, saturation pressure (vaporous cavitation), and air solubility (gaseous cavitation) were compared. The simulation results revealed that the gaseous cavitation model showed little improvement in accuracy compared with the other cavitation models, with regard to load and temperature prediction.

5.3 Computational Fluid Dynamics Modeling: Tilting Pad Journal Bearing TPJB. Computational fluid dynamics based models for TPJB [42–44,129–131,138–142,145] first appeared in the literature mainly in the period 2014–2019. Most of the studies [42,129,130,138–140,142,145] only considered a single pad due to the heavy computational load, although several modeled the full tilting pad journal bearing [43,44,131,141]. Edney et al. [138] modeled a 2D slice of a single pad with a LEG and focused mainly on thermal and turbulence flow. The *k*-epsilon turbulence model was applied, and the effects of the leading-edge geometrical parameters were investigated. The addition of a taper at the exit of the LEG showed a significant impact on the pressure distribution. A recirculation zone that affects pad inlet temperature was observed in the LEG.

Armentrout et al. [139] investigated the influence of turbulence and fluid inertia in a water lubricated bearing, utilizing a 3D single pad model that did not include groove mixing physics. A conventional approach was utilized to obtain the shaft and pad equilibrium positions. The *k-w* turbulence model was used, and the effects of turbulence and fluid inertia were around 50% and 6%, respectively, on the value of the load capacity. The authors mentioned that the thermal effect was not included due to the low viscosity and high specific heat of the water lubrication. It was concluded that the accuracy of the turbulence and fluid inertia in the Reynolds model could be improved by adjusting the empirical constant based on the CFD solution.

Hagemann et al. [42,129,130] and Hagemann and Schwarze [140] presented a TPJB model for a single pad with a LEG and focused mainly on the 3D thermal and turbulence (*k-w*) models, and flow coupling with the rigid pad. The equilibrium positions of the shaft and pad were obtained from an iterative calculation process in the CFD solver. In the study [129], the pressures from an experiment and from the CFD simulation were significantly increased at the leading edge, just after passing through the groove region, due to the fluid inertia effect. This significantly affected the pressure distribution on the pad region. In addition, a simplified energy approach was combined with the Reynolds model to consider the sudden increase of the pressure at the leading edge. The heat transfer coefficient effect on the pad surfaces was examined for the LEG type TPJB in Hagemann [42]. This showed a significant influence on the maximum pad temperature. The modeling techniques for the heat transfer coefficient of the pad surfaces were later utilized by the authors in the development of an advanced Reynolds-based bearing code [140]. Crone et al. [145] carried out a comparative CFD study between flooded and LEG type TPJB. The model only included a single rigid pad and adopted the shear stress transport (SST) turbulence model with the 3D energy equation. The LEG type TPJB showed a higher maximum pad temperature due to the heightened turbulence effect in the flooded type bearing.

Ding et al. [131,141] compared 14 turbulence models, under super-laminar flow regime, for a single pad bearing model. By comparing simulation and experimental results, they concluded that a low-Re correction for the SST is the best model for the super-laminar flow. Li et al. [142] proposed a dynamic mesh algorithm to accommodate shaft-pad motions, without the loss of the orthogonal mesh quality. The algorithm is suitable when predicting the dynamic behavior of the rotor-bearing system in FLUENT. Ding et al. [141] analyzed air entrainment and thermal effects for a large-scale full TPJB. The results revealed that air entrainment is an essential factor for accurate prediction of friction power loss in unloaded pads.

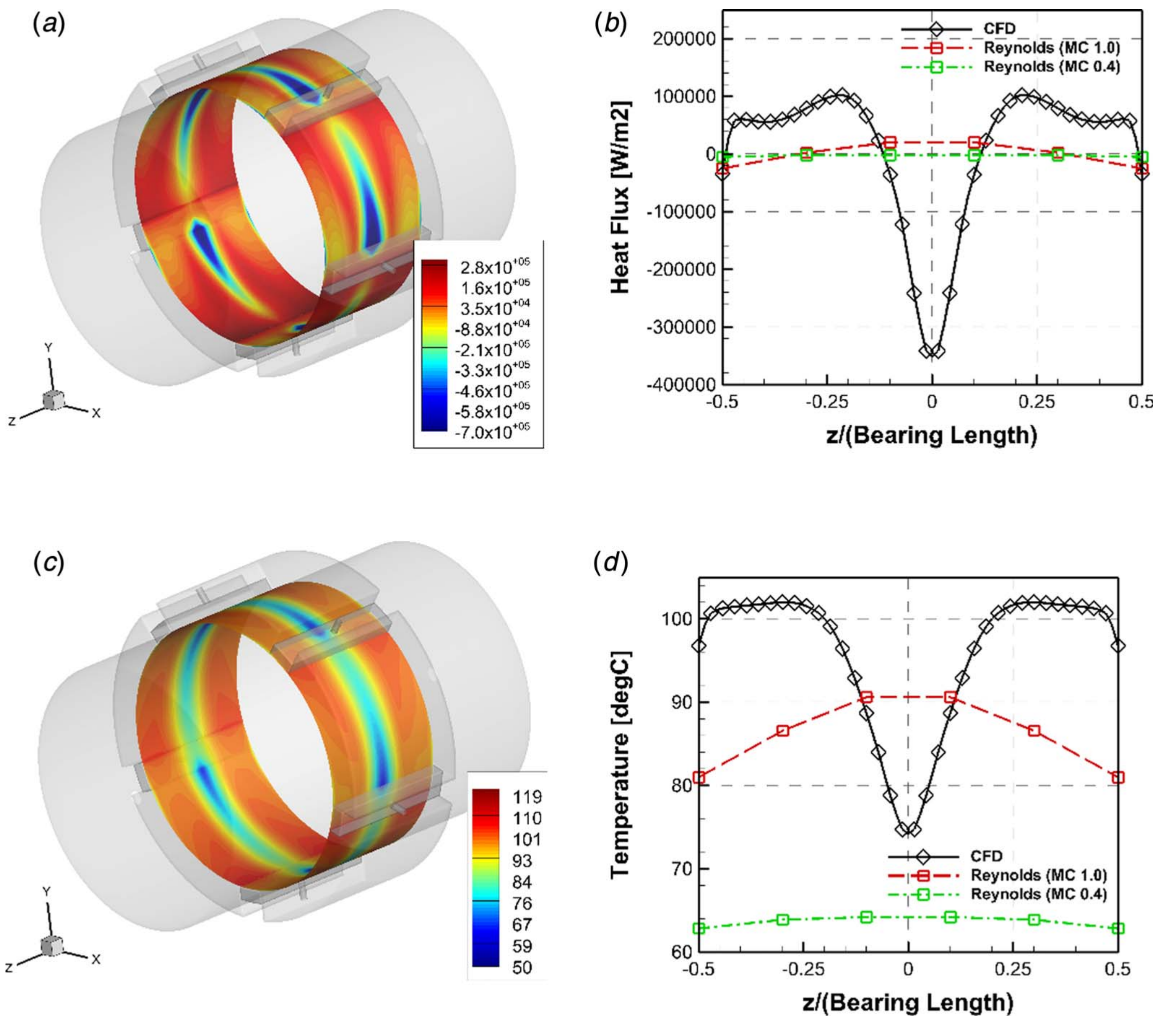

Fig. 10 Heat with mixing effect: (*a*) heat flux [W/m^2], (*b*) circumferentially averaged heat flux distribution, (c) temperature flux and temperature at shaft surface [°C], and (*d*) circumferentially averaged temperature distribution [43]

Yang and Palazzolo [43,44,160,161] presented a CFD based TEHD modeling approach for obtaining static and dynamic responses, utilizing a coupled, full TPJB model. This brought TPJB CFD modeling up to the most advanced conventional Reynolds models, in terms of included features. Their model included incompressible multiphase flow, thermal-fluid coupling, transitional turbulence, thermal shaft-pad deformations, pivot flexibility, shaft-pad equilibrium determination, and frequency reduced dynamic coefficients. Mesh deformation equations were provided to maintain the orthogonal mesh quality for all shaft and pad motions. The researchers revealed the importance of modeling the between BP regions with oil inlets, by comparing response results between Reynolds and CFD models. The Reynolds model utilized an approximate mixing coefficient MC to account for the thermal mixing between pads BP, whereas the CFD model included the detailed BP geometry. Response results varied widely between the MC equals 0.4 and MC equals 1.0 cases. The Reynolds with MC model predicted dynamic coefficients considerably different from their CFD predicted counterparts. A major cause of the difference was discovered to be the radial and axial temperature distributions at the pad inlet were ignored in the Reynolds-mixing theory approach. The radial temperature distribution was confirmed from the heat flux results in Figs. 10(*a*) and 10(*b*). As shown in Figs. 10(*c*) and 10(*d*), the existence of the axial temperature distribution was observed. Also, the CFD model in the research predicted higher damping coefficients, and it corresponded to the results in the previous CFD study [127].

6 Conclusion

An extensive survey of publications on thermal effects on bearing dynamic and static performances, thermal instability problems was presented. The important findings of the surveys are as follows:

- High-fidelity thermal effect models including 3D temperature distributions of the fluid film, shaft, and bearing structures have been developed.
- Transient simulations of high-fidelity models of journal bearings including thermal effects have been performed with the advances in high-performance computing.
- More accurate models of journal bearing inlet temperatures resulting from thermal flow mixing have been developed, with significant effects on temperature distributions.
- The thermal bow instability problems (Morton effect) are more frequently observed due to the high operating speed and power density in modern turbomachinery.
- High-fidelity Morton effect models including the 3D energy equation and detailed thermal rotor structures have been developed and correlated well with available test data.
- Significant progress on thermal modeling of gas-lubricated journal bearing has been made.
- Thermal instability problems in gas journal bearings recently have gained much attention. The experimental and theoretical works to handle those instability problems have been conducted.

— There has been significant progress in the CFD analysis of the thermal effects in plain journal bearings, and the CFD analysis has been extended to the tilting pad journal bearing modeling recently.
— By comparison with CFD models, it appears that the Reynolds equation approach using pad inlet temperatures based on mixing coefficients may be unreliable in some cases.

Acknowledgment

The authors gratefully acknowledge the financial support on this research from the Texas A&M Turbomachinery Research Consortium (TRC).

Conflict of Interest

There are no conflicts of interest.

References

[1] Knight, J. D., and Niewiarowski, A. J., 1990, "Effects of Two Film Rupture Models on the Thermal Analysis of a Journal Bearing," ASME J. Tribol., **112**(2), pp. 183–188.
[2] Taniguchi, S., Makino, T., Takeshita, K., and Ichimura, T., 1990, "A Thermohydrodynamic Analysis of Large Tilting-Pad Journal Bearing in Laminar and Turbulent Flow Regimes With Mixing," ASME J. Tribol., **112**(3), pp. 542–548.
[3] Knight, J. D., and Ghadimi, P., 1992, "Effects of Modified Effective Length Models of the Rupture Zone on the Analysis of a Fluid Journal Bearing," STLE Tribol. Trans., **35**(1), pp. 29–36.
[4] Simmons, J. E. L., and Dixon, S. J., 1994, "Effect of Load Direction, Preload, Clearance Ratio and Oil Flow on the Performance of a 200mm Journal Pad Bearing," STLE Tribol. Trans., **37**(2), pp. 227–236.
[5] Kim, J., Palazzolo, A. B., and Gadangi, R. K., 1994, "TEHD Analysis for Tilting Pad Journal Bearings Using Upwind Finite Element Method," Tribol. Trans., **37**(4), pp. 771–783.
[6] Suh, J., and Palazzolo, A., 2015, "Three-Dimensional Dynamic Model of TEHD Tilting-Pad Journal Bearing—Part I: Theoretical Modeling," ASME J. Tribol., **137**(4), p. 041703.
[7] Ettles, C., 1969, "Hot Oil Carry-Over in Thrust Bearings," Proc. Instin. Mech. Eng. Conf. Proc., **184**(12), pp. 75–81.
[8] Mitsui, J., Hori, Y., and Tanaka, M., 1983, "Thermohydrodynamic Analysis of Cooling Effect of Supply Oil in Circular Journal Bearings," ASME J. Tribol., **105**(3), pp. 414–421.
[9] Kim, J., Palazzolo, A., and Gadangi, R., 1995, "Dynamic Characteristics of TEHD Tilt Pad Journal Bearing Simulation Including Multiple Mode Pad Flexibility Model," ASME J. Vib. Acoust., **117**(1), pp. 123–135.
[10] Gadangi, R. K., and Palazzolo, A. B., 1995, "Transient Analysis of Tilt Pad Journal Bearings Including Effects of Pad Flexibility and Fluid Film Temperature," ASME J. Tribol., **117**(2), pp. 302–307.
[11] Desbordes, H., Fillon, M., Frêne, J., and Chan Hew Wai, C., 1995, "The Effects of Three-Dimensional Pad Deformations on Tilting-Pad Journal Bearings Under Dynamic Loading," ASME J. Tribol., **117**(3), pp. 379–384.
[12] Fillon, M., Desbordes, H., Frêne, J., and Chan Hew Wai, C., 1996, "A Global Approach of Thermal Effects Including Pad Deformations in Tilting-Pad Journal Bearings Submitted to Unbalance Load," ASME J. Tribol., **118**(1), pp. 169–174.
[13] Gadangi, R. K., Palazzolo, A. B., and Kim, J., 1996, "Transient Analysis of Plain and Tilt Pad Journal Bearings Including Fluid Film Temperature Effects," ASME J. Tribol., **118**(2), pp. 423–430.
[14] Monmousseau, P., and Fillon, M., 1999, "Frequency Effects on the TEHD Behavior of a Tilting-Pad Journal Bearing Under Dynamic Loading," ASME J. Tribol., **121**(2), pp. 321–326.
[15] Gandjalikhan Nassab, S. A., and Maoyeri, M. S., 2002, "Three-dimensional Thermohydrodynamic Analysis of Axially Grooved Journal Bearings," Proc. Inst. Mech. Eng., Part J, **216**(1), pp. 35–47.
[16] Nicholas, J. C., 2003, "Tilting Pad Bearings With Spray-Bar Blockers and By-Pass Cooling for High Speed, High Load Applications," Proceedings of 32rd Turbomachinery Symposium, Texas A&M University, pp. 27–37.
[17] He, M., Allaire, P., Cloud, C. H., and Nicholas, J., 2004, "A Pressure Dam Bearing Analysis With Adiabatic Thermal Effects," Tribol. Trans., **47**(1), pp. 70–76.
[18] Fatu, A., Hajjam, M., and Bonneau, D., 2005, "A New Model of Thermoelastohydrodynamic Lubrication in Dynamically Loaded Journal Bearings," ASME J. Tribol., **128**(1), pp. 85–95.
[19] Brito, F. P., Miranda, A. S., Bouyer, J., and Fillon, M., 2006, "Experimental Investigation of the Influence of Supply Temperature and Supply Pressure on the Performance of a Two-Axial Groove Hydrodynamic Journal Bearing," ASME J. Tribol., **129**(1), pp. 98–105.
[20] Liu, D., Zhang, W., and Zheng, T., 2007, "A Simplified One-Dimensional Thermal Model for Journal Bearings," ASME J. Tribol., **130**(1), p. 011003.
[21] Sim, K., and Kim, D., 2008, "Thermohydrodynamic Analysis of Compliant Flexure Pivot Tilting Pad Gas Bearings," ASME J. Eng. Gas Turbines Power, **130**(3), p. 032502.
[22] Bang, K. B., Kim, J. H., and Cho, Y. J., 2010, "Comparison of Power Loss and Pad Temperature for Leading Edge Groove Tilting Pad Journal Bearings and Conventional Tilting Pad Journal Bearings," Tribol. Int., **43**(8), pp. 1287–1293.
[23] Chauhan, A., Sehgal, R., and Sharma, R. K., 2011, "Investigations on the Thermal Effects in Non-Circular Journal Bearings," Tribol. Int., **44**(12), pp. 1765–1773.
[24] Solghar, A. A., Brito, F. P., Claro, J. C. P., and Nassab, S. A. G., 2011, "An Experimental Study of the Influence of Loading Direction on the Thermohydrodynamic Behavior of Twin Axial Grooves Journal Bearings," J. Eng. Tribol., **225**(5), pp. 245–254.
[25] Thorat, M. R., Pettinato, B. C., and De Choudhury, P., 2014, "Metal Temperature Correlations in Tilting Pad Journal Bearings," ASME J. Eng. Gas Turbines Power, **136**(11), p. 112503.
[26] Tschoepe, D. P., and Childs, D. W., 2014, "Measurements Versus Predictions for the Static and Dynamic Characteristics of a Four-Pad, Rocker-Pivot, Tilting-Pad Journal Bearing," ASME J. Eng. Gas Turbines Power, **136**(5), p. 052501.
[27] Suh, J., and Palazzolo, A., 2015, "Three-Dimensional Dynamic Model of TEHD Tilting-Pad Journal Bearing—Part II: Parametric Studies," ASME J. Tribol., **137**(4), p. 041704.
[28] Zhang, F., Ouyang, W., Hong, H., Guan, Y., Yuan, X., and Dong, G., 2015, "Experimental Study on Pad Temperature and Film Thickness of Tilting-Pad Journal Bearings With an Elastic-Pivot Pad," Tribol. Int., **88**, pp. 228–235.
[29] Kuznetsov, E., and Glavatskih, S., 2016, "Dynamic Characteristics of Compliant Journal Bearings Considering Thermal Effects," Tribol. Int., **94**, pp. 288–305.
[30] Li, H., Yin, Z., and Wang, Y., 2019, "Study on the Performance of Journal Bearings in Different Lubricants by CFD and FSI Method With Thermal Effect and Cavitation," MATEC Web of Conferences, Orlando, FL, Oct. 13–15, 2018.
[31] Mo, J., Gu, C., Pan, X., Zheng, S., and Ying, G., 2017, "A Thermohydrodynamic Analysis of the Self-Lubricating Bearings Applied in Gear Pumps Using Computational Fluid Dynamics Method," ASME J. Tribol., **140**(1), p. 011102.
[32] Nichols, B. R., Fittro, R. L., and Goyne, C. P., 2018, "Steady-State Tilting-Pad Bearing Performance Under Reduced Oil Supply Flow Rates," ASME J. Tribol., **140**(5), p. 051701.
[33] Bouyer, J., Fillon, M., Helene, M., Beaurain, J., and Giraudeau, C., 2018, "Behavior of a Two-Lobe Journal Bearing With a Scratched Shaft: Comparison Between Theory and Experiment," ASME J. Tribol., **141**(2), p. 021702.
[34] Bouyer, J., and Fillon, M., 2001, "An Experimental Analysis of Misalignment Effects on Hydrodynamic Plain Journal Bearing Performances," ASME J. Tribol., **124**(2), pp. 313–319.
[35] El-Butch, A. M., and Ashour, N. M., 2005, "Transient Analysis of Misaligned Elastic Tilting Pad Journal Bearing," Tribol. Int., **38**(1), pp. 41–48.
[36] Jang, J. Y., and Khonsari, M. M., 2009, "On the Behavior of Misaligned Journal Bearings Based on Mass-Conservative Thermohydrodynamic Analysis," ASME J. Tribol., **132**(1), p. 011702.
[37] Sun, J., Deng, M., Fu, Y., and Gui, C., 2009, "Thermohydrodynamic Lubrication Analysis of Misaligned Plain Journal Bearing With Rough Surface," ASME J. Tribol., **132**(1), p. 011704.
[38] Suh, J., and Choi, Y.-S., 2016, "Pivot Design and Angular Misalignment Effects on Tilting Pad Journal Bearing Characteristics: Four Pads for Load on Pad Configuration," Tribol. Int., **102**, pp. 580–599.
[39] Yang, P., Yuan, Q., and Chen, R., 2018, "Experimental Research on the Tilting Pad Bearing Under the High Temperature of Inlet Oil," Ind. Lubr. Tribol., **70**(6), pp. 935–941.
[40] Abdollahi, B., and San Andrés, L., 2018, "Improved Estimation of Bearing Pads' Inlet Temperature: A Model for Lubricant Mixing at Oil Feed Ports and Validation Against Test Data," ASME J. Tribol., **141**(3), p. 031703.
[41] Hagemann, T., and Schwarze, H., 2018, "A Model for Oil Flow and Fluid Temperature Inlet Mixing in Hydrodynamic Journal Bearings," ASME J. Tribol., **141**(2), p. 021701.
[42] Hagemann, T., Zeh, C., and Schwarze, H., 2019, "Heat Convection Coefficients of a Tilting-pad Journal Bearing With Directed Lubrication," Tribol. Int., **136**, pp. 114–126.
[43] Yang, J., and Palazzolo, A., 2019, "Three-Dimensional Thermo-Elasto-Hydrodynamic Computational Fluid Dynamics Model of a Tilting Pad Journal Bearing—Part I: Static Response," ASME J. Tribol., **141**(6), p. 061702.
[44] Yang, J., and Palazzolo, A., 2019, "Three-Dimensional Thermo-Elasto-Hydrodynamic Computational Fluid Dynamics Model of a Tilting Pad Journal Bearing—Part II: Dynamic Response," ASME J. Tribol., **141**(6), p. 061703.
[45] Morton, P. G., 1975, "Some Aspects of Thermal Instability in Generators," G.E.C. Internal Report No. S/W40 u183.
[46] Hesseborn, B., 1978, "Measurements of Temperature Unsymmetries in Bearing Journal Due to Vibration," Internal Report ABB Stal.
[47] Dimarogonas, A., 1974, "A Study of the Newkirk Effect in Turbomachinery," Wear, **28**(3), pp. 369–382.
[48] Kellenberger, W., 1980, "Spiral Vibrations Due to the Seal Rings in Turbogenerators Thermally Induced Interaction Between Rotor and Stator," ASME J. Mech. Des., **102**(1), pp. 177–184.
[49] Newkirk, B., 1927, "Shaft Rubbing," J. Am. Soc. Nav. Eng., **39**(1), pp. 114–120.

[50] Schmied, J., 1987, "Spiral Vibrations of Rotors," *Rotating Machinery Dynamics*, A. Muszynska, and J. C. Simonis, eds., Vol. 2, ASME, New York.
[51] Standard, A., 2005, *Tutorial on Rotordynamics: Lateral Critical, Unbalance Response, Stability, Train Torsional and Rotor Balancing*, 2nd ed., American Petroleum Institute, Washington, DC, 684.
[52] de Jongh, F., 2008, "The Synchronous Rotor Instability Phenomenon—Morton Effect," 37th Turbomachinery Symposium, Houston, TX, Sept. 8–11, pp. 159–167.
[53] Gu, L., 2018, "A Review of Morton Effect: From Theory to Industrial Practice," Tribol. Trans., **61**(2), pp. 381–391.
[54] Tong, X., Palazzolo, A., and Suh, J., 2017, "A Review of the Rotordynamic Thermally Induced Synchronous Instability (Morton) Effect," ASME Appl. Mech. Rev., **69**(6), p. 060801.
[55] de Jongh, F., and Van Der Hoeven, P., 1998, "Application of a Heat Barrier Sleeve to Prevent Synchronous Rotor Instability," 27th Turbomachinery Symposium, Houston, TX, Sept. 20–24, pp. 17–26.
[56] Schmied, J., Pozivil, J., and Walch, J., 2008, "Hot Spots in Turboexpander Bearings: Case History, Stability Analysis, Measurements and Operational Experience," ASME Paper No. GT2008-51179.
[57] Marscher, W., and Illis, B., 2007, "Journal Bearing Morton Effect Cause of Cyclic Vibration in Compressors," Tribol. Trans., **50**(1), pp. 104–113.
[58] Berot, F., and Dourlens, H., 1999, "On Instability of Overhung Centrifugal Compressors," ASME Paper No. 99-GT-202.
[59] de Jongh, F., and Morton, P., 1994, "The Synchronous Instability of a Compressor Rotor Due to Bearing Journal Differential Heating," ASME Paper No. 94-GT-035.
[60] Kocur, J., and de Jongh, F., 2000, "Thermal Rotor Instability in Gas Compressors," 14th International Gas Convention, Caracas, Venezuela, May 10–12, pp. 1–14.
[61] Corcoran, J., Rea, H., Cornejo, G., and Leonhard, M., 1997, "Discovering, the Hard Way, How a High Performance Coupling Influenced the Critical Speeds and Bearing Loading of an Overhung Radial Compressor—A Case History," 26th Turbomachinery Symposium, Houston, TX, Sept., pp. 67–78.
[62] Kirk, G., Guo, Z., and Balbahadur, A., 2003, "Synchronous Thermal Instability Prediction for Overhung Rotors," 32nd Turbomachinery Symposium, Houston, TX, Sept. 8–11, pp. 121–135.
[63] Kirk, G., and Guo, Z., 2013, "Design Tool for Prediction of Thermal Synchronous Instability," ASME Paper No. DETC2013-12966.
[64] Tong, X., and Palazzolo, A., 2016, "Double Overhung Disk and Parameter Effect on Rotordynamic Synchronous Instability—Morton Effect—Part I: Theory and Modeling Approach," ASME J. Tribol., **139**(1), p. 011705.
[65] Childs, D., and Saha, R., 2012, "A New, Iterative, Synchronous-Response Algorithm for Analyzing the Morton Effect," ASME J. Eng. Gas Turbines Power, **134**(7), p. 072501.
[66] Faulkner, H., Strong, W., and Kirk, R., 1997, "Thermally Induced Synchronous Instability of a Radial Inflow Overhung Turbine—Part II," ASME Design Engineering Technical Conference, Sacramento, CA, Sept. 14–17, Paper No. DETC97/VIB-4174.
[67] Lorenz, J., and Murphy, B., 2011, "Case Study of Morton Effect Shaft Differential Heating in a Variable-Speed Rotating Electric Machine," ASME Paper No. GT2011-45228.
[68] Suh, J., and Palazzolo, A., 2014, "Three-Dimensional Thermohydrodynamic Morton Effect Analysis—Part II: Parametric Studies," ASME J. Tribol., **136**(3), p. 031707.
[69] Balbahadur, A., 2001, "A Thermoelastohydrodynamic Model of the Morton Effect Operating in Overhung Rotors Supported by Plain or Tilting Pad Journal Bearings," Ph.D. thesis, Virginia Tech, Blacksburg, VA.
[70] Panara, D., Panconi, S., and Griffini, D., 2015, "Numerical Prediction and Experimental Validation of Rotor Thermal Instability," 44th Turbomachinery Symposium, Houston, TX, Sept. 14–17.
[71] Tong, X., and Palazzolo, A., 2017, "Measurement and Prediction of the Journal Circumferential Temperature Distribution for the Rotordynamic Morton Effect," ASME J. Tribol., **140**(3), p. 031702.
[72] Keogh, P., and Morton, P., 1993, "Journal Bearing Differential Heating Evaluation With Influence on Rotor Dynamic Behaviour," Proc. R. Soc. London, Ser. A, **441**(1913), pp. 527–548.
[73] Keogh, P., and Morton, P., 1994, "The Dynamic Nature of Rotor Thermal Bending Due to Unsteady Lubricant Shearing Within a Bearing," Proc. R. Soc. London, Ser. A, **445**(1924), pp. 273–290.
[74] Larsson, B., 1999, "Journal Asymmetric Heating—Part I: Nonstationary Bow," ASME J. Tribol., **121**(1), pp. 157–163.
[75] Larsson, B., 1999, "Journal Asymmetric Heating—Part II: Alteration of Rotor Dynamic Properties," ASME J. Tribol., **121**(1), pp. 164–168.
[76] Tucker, P., and Keogh, P., 1996, "On the Dynamic Thermal State in a Hydrodynamic Bearing With a Whirling Journal Using CFD Techniques," ASME J. Tribol., **118**(2), pp. 356–363.
[77] Gomiciaga, R., and Keogh, P., 1999, "Orbit Induced Journal Temperature Variation in Hydrodynamic Bearings," ASME J. Tribol., **121**(1), pp. 77–84.
[78] Murphy, B., and Lorenz, J., 2010, "Simplified Morton Effect Analysis for Synchronous Spiral Instability," ASME J. Vib. Acoust., **132**(5), p. 051008.
[79] Lee, J., and Palazzolo, A., 2012, "Morton Effect Cyclic Vibration Amplitude Determination for Tilt Pad Bearing Supported Machinery," ASME J. Tribol., **135**(1), p. 011701.
[80] Grigor'ev, B. S., Fedorov, A. E., and Schmied, J., 2015, "New Mathematical Model for the Morton Effect Based on the THD Analysis," Nineth IFToMM International Conference on Rotor Dynamics, Milan, Italy, Sept. 22–25, pp. 2243–2253.
[81] Tong, X., Palazzolo, A., and Suh, J., 2016, "Rotordynamic Morton Effect Simulation With Transient, Thermal Shaft Bow," ASME J. Tribol., **138**(3), p. 031705.
[82] Tong, X., and Palazzolo, A., 2016, "Double Overhung Disk and Parameter Effect on Rotordynamic Synchronous Instability—Morton Effect—Part II: Occurrence and Prevention," ASME J. Tribol., **139**(1), p. 011706.
[83] Tong, X., and Palazzolo, A., 2018, "Tilting Pad Gas Bearing Induced Thermal Bow-Rotor Instability," Tribol. Int., **121**, pp. 269–279.
[84] Khonsari, M., and Beaman, J., 1986, "Thermohydrodynamic Analysis of Laminar Incompressible Journal Bearings," ASLE Trans., **29**(2), pp. 141–150.
[85] Knight, J. D., and Barrett, L. E., 1988, "Analysis of Tilting Pad Journal Bearings With Heat Transfer Effects," ASME J. Tribol., **110**(1), pp. 128–133.
[86] Fillon, M., Bligoud, J., and Frêne, J., 1992, "Experimental Study of Tilting-Pad Journal Bearings—Comparison With Theoretical Thermoelastohydrodynamic Results," ASME J. Tribol., **114**(3), pp. 579–587.
[87] He, M., Allaire, P., Barrett, L., and Nicholas, J., 2005, "Thermohydrodynamic Modeling of Leading-Edge Groove Bearings Under Starvation Condition," Tribol. Trans., **48**(3), pp. 362–369.
[88] Suh, J., and Palazzolo, A., 2014, "Three-Dimensional Thermohydrodynamic Morton Effect Simulation—Part I: Theoretical Model," ASME J. Tribol., **136**(3), p. 031706.
[89] San Andrés, L., Ryu, K., and Kim, T. H., 2010, "Identification of Structural Stiffness and Energy Dissipation Parameters in a Second Generation Foil Bearing: Effect of Shaft Temperature," ASME J. Eng. Gas Turbines Power, **133**(3), p. 032501.
[90] Salehi, M., and Heshmat, H., 2000, "On the Fluid Flow and Thermal Analysis of a Compliant Surface Foil Bearing and Seal," Tribol. Trans., **432**(2), pp. 318–324.
[91] Salehi, M., Swanson, E., and Heshmat, H., 2000, "Thermal Features of Compliant Foil Bearings—Theory and Experiments," ASME J. Tribol., **123**(3), pp. 566–571.
[92] Kim, T. H., and San Andrés, L., 2009, "Thermohydrodynamic Model Predictions and Performance Measurements of Bump-Type Foil Bearing for Oil-Free Turboshaft Engines in Rotorcraft Propulsion Systems," ASME J. Tribol., **132**(1), p. 011701.
[93] Peng, Z., and Khonsari, M. M., 2006, "A Thermohydrodynamic Analysis of Foil Journal Bearings," ASME J. Tribol., **128**(3), pp. 534–541.
[94] Lee, D., and Kim, D., 2010, "Thermohydrodynamic Analyses of Bump Air Foil Bearings With Detailed Thermal Model of Foil Structures and Rotor," ASME J. Tribol., **132**(2), p. 021704.
[95] Sim, K., and Kim, T. H., 2012, "Thermohydrodynamic Analysis of Bump-Type Gas Foil Bearings Using Bump Thermal Contact and Inlet Flow Mixing Models," Tribol. Int., **48**, pp. 137–148.
[96] Gita, T., and Carpino, M., 2011, "Thermal Structural Effects in a Gas-Lubricated Foil Journal Bearing," Tribol. Trans., **54**(5), pp. 701–713.
[97] Lehn, A., Mahner, M., and Schweizer, B., 2017, "A Contribution to the Thermal Modeling of Bump Type Air Foil Bearings: Analysis of the Thermal Resistance of Bump Foils," ASME J. Tribol., **139**(6), p. 061702.
[98] Paouris, L. I., Bompos, D. A., and Nikolakopoulos, P. G., 2013, "Simulation of Static Performance of Air Foil Bearings Using Coupled Finite Element and Computational Fluid Dynamics Techniques," ASME J. Eng. Gas Turbines Power, **136**(2), p. 022503.
[99] Aksoy, S., and Aksit, M. F., 2015, "A Fully Coupled 3D Thermo-Elastohydrodynamics Model for a Bump-Type Compliant Foil Journal Bearing," Tribol. Int., **82**, pp. 110–122.
[100] Lee, D., and Kim, D., 2011, "Three-Dimensional Thermohydrodynamic Analyses of Rayleigh Step Air Foil Thrust Bearing With Radially Arranged Bump Foils," Tribol. Trans., **54**(3), pp. 432–448.
[101] Gad, A. M., and Kaneko, S., 2015, "Tailoring of the Bearing Stiffness to Enhance the Performance of Gas-Lubricated Bump-Type Foil Thrust Bearing," Proc. Inst. Mech. Eng., Part J, **230**(5), pp. 541–560.
[102] Lehn, A., Mahner, M., and Schweizer, B., 2018, "A Thermo-Elasto-Hydrodynamic Model for Air Foil Thrust Bearings Including Self-Induced Convective Cooling of the Rotor Disk and Thermal Runaway," Tribol. Int., **119**, pp. 281–298.
[103] Qin, K., Peter, A. J., Joshua, A. K., Li, D., and Jahn, I., 2018, "A Fluid-Structure-Thermal Model for Bump-Type Foil Thrust Bearings," Tribol. Int., **121**, pp. 481–491.
[104] Feng, K., Li, W., Deng, Z., and Zhang, M., 2017, "Thermohydrodynamic Analysis and Thermal Management of Spherical Spiral Groove gas Bearings," Tribol. Trans., **60**(4), pp. 629–644.
[105] Zhang, K., Zhao, X., Feng, K., and Zhao, Z., 2018, "Thermohydrodynamic Analysis and Thermal Management of Hybrid Bump–Metal Mesh Foil Bearings: Experimental Tests and Theoretical Predictions," Int. J. Therm. Sci., **127**, pp. 91–104.
[106] Feng, K., and Kaneko, S., 2009, "Thermohydrodynamic Study of Multiwound Foil Bearing Using Lobatto Point Quadrature," ASME J. Tribol., **131**(2), p. 021702.
[107] Kim, D., 2015, "Design Space of Foil Bearings for Closed-Loop Supercritical CO_2 Power Cycles Based on Three-Dimensional Thermohydrodynamic Analyses," ASME J. Eng. Gas Turbines Power, **138**(3), p. 032504.
[108] Chien, S.-Y., Cramer, M., and Untaroiu, A., 2017, "A Compressible Thermohydrodynamic Analysis of Journal Bearings Lubricated With Supercritical CO2," Proceedings of the ASME 2017 Fluids Engineering Division Summer Meeting. Volume 1B, Symposia: Fluid Measurement and

Instrumentation; Fluid Dynamics of Wind Energy; Renewable and Sustainable Energy Conversion; Energy and Process Engineering; Microfluidics and Nanofluidics; Development and Applications in Computational Fluid Dynamics; DNS/LES and Hybrid RANS/LES Methods, Waikoloa, HI, July 30–Aug. 3, p. V01BT09A001.

[109] Lee, D., Kim, D., and Sadashiva, R. P., 2011, "Transient Thermal Behavior of Preloaded Three-Pad Foil Bearings: Modeling and Experiments," ASME J. Tribol., **133**(2), p. 021703.

[110] Samanta, P., and Khonsari, M. M., 2018, "On the Thermoelastic Instability of Foil Bearings," Tribol. Int., **121**, pp. 10–20.

[111] DellaCorte, C., 1998, "A New Foil Air Bearing Test Rig for Use to 700 °C and 70,000 rpm," STLE Tribol. Trans., **41**(3), pp. 335–340.

[112] DellaCorte, C., Valco, M. J., Radil, K. C., Heshmat, H., and Lukaszewicz, V. L., 2000, "Performance and Durability of High Temperature Foil Air Bearings for Oil-Free Turbomachinery," Tribol. Trans., **43**(4), pp. 774–780.

[113] Radil, K., and Zeszotek, M., 2004, "An Experimental Investigation Into the Temperature Profile of a Compliant Foil Air Bearing," Tribol. Trans., **47**(4), pp. 470–479.

[114] Zywica, G., Baginski, P., and Banaszek, S., 2015, "Experimental Studies on Foil Bearing With a Sliding Coating Made of Synthetic Material," ASME J. Tribol., **138**(1), p. 011301.

[115] Abraham Chirathadam, T., and San Andrés, L., 2013, "Measurements of Rotordynamic Response and Temperatures in a Rotor Supported on Metal Mesh Foil Bearings," ASME J. Eng. Gas Turbines Power, **135**(12), p. 122507.

[116] Howard, S. A., DellaCorte, C., Valco, M. J., Prahl, J. M., and Heshmat, H., 2001, "Steady-State Stiffness of Foil Air Journal Bearings at Elevated Temperatures," Tribol. Trans., **44**(3), pp. 489–493.

[117] Howard, S., DellaCorte, C., Valco, M. J., Prahl, J. M., and Heshmat, H., 2001, "Dynamic Stiffness and Damping Characteristics of a High-Temperature Air Foil Journal Bearing," Tribol. Trans., **44**(4), pp. 657–663.

[118] Kim, T. H., Breedlove, A. W., and San Andrés, L., 2009, "Characterization of a Foil Bearing Structure at Increasing Temperatures: Static Load and Dynamic Force Performance," ASME J. Tribol., **131**(4), p. 041703.

[119] Dykas, B., and Howard, S. A., 2004, "Journal Design Considerations for Turbomachine Shafts Supported on Foil Air Bearings," STLE Tribol. Trans., **47**(4), pp. 508–516.

[120] Ryu, K., and Andrés, L. S., 2012, "Effect of Cooling Flow on the Operation of a Hot Rotor-Gas Foil Bearing System," ASME J. Eng. Gas Turbines Power, **134**(10), p. 102511.

[121] Żywica, G., Bagiński, P., and Kiciński, J., 2017, "Selected Operational Problems of High-Speed Rotors Supported by Gas Foil Bearings," Technische Mechanik, **37**(2–5), pp. 339–346.

[122] Radil, K., Howard, S., and Dykas, B., 2002, "The Role of Radial Clearance on the Performance of Foil Air Bearings," STLE Tribol. Trans., **454**(4), pp. 485–490.

[123] Radil, K., DellaCorte, C., and Zeszotek, M., 2007, "Thermal Management Techniques for Oil-Free Turbomachinery Systems," STLE Tribol. Trans., **50**(3), pp. 319–327.

[124] Radil, K. C., and DellaCorte, C., 2009, "A Three-Dimensional Foil Bearing Performance Map Applied to Oil-Free Turbomachinery," Tribol. Trans., **53**(5), pp. 771–778.

[125] Ryu, K., and San Andrés, L., 2013, "On the Failure of a Gas Foil Bearing: High Temperature Operation Without Cooling Flow," ASME J. Eng. Gas Turbines Power, **135**(11), p. 112506.

[126] Sim, K., Lee, Y., Song, J., and Kim, T., 2018, "Effect of Cooling Flow on Thermal Performance of a Gas Foil Bearing Floating on a Hot Rotor," J. Mech. Sci. Technol., **32**(5), pp. 1939–1954.

[127] Guo, Z., Toshio, H., and Gorden, R., 2005, "Application of CFD Analysis for Rotating Machinery Part 1: Hydrodynamic, Hydrostatic Bearings and Squeeze Film Damper," ASME J. Eng. Gas Turbines Power, **4**(2), pp. 445–451.

[128] Uhkoetter, S., aus der Wiesche, S., Kursch, M., and Beck, C., 2012, "Development and Validation of a Three-Dimensional Multiphase Flow CFD Analysis for Journal Bearings in Steam and Heavy Duty Gas Turbines," Proceedings of the ASME Turbo Expo 2012: Turbine Technical Conference and Exposition. Volume 7: Structures and Dynamics, Parts A and B, Copenhagen, Denmark. June 11–15, pp. 749–758.

[129] Hagemann, T., Zeh, C., Pr€olß, M., and Schwarze, H., 2017, "The Impact of Convective Fluid Inertia Forces on Operation of Tilting-Pad Journal Bearings," Int. J. Rotating Mach., **2017**, pp. 1–12.

[130] Hagemann, T., Pfeiffer, P., and Schwarze, H., 2018, "Measured and Predicted Operating Characteristics of a Tilting-Pad Journal Bearing With Jacking-Oil Device at Hydrostatic, Hybrid, and Hydrodynamic Operation," Lubricants, **6**(3), p. 81.

[131] Ding, A., Ren, X., Li, X., and Gu, C., 2018, "Numerical Investigation of Turbulence Models for a Superlaminar Journal Bearing," Adv. Tribol., **2018**, p. 1–14.

[132] Heshmat, H., and Pinkus, O., 1989, "Workshop on Thermal Aspects of Fluid Film Lubrication—A Summary," ASME J. Tribol., **111**(4), pp. 567–568.

[133] Tucker, P., and Keogh, P., 1994, "A Generalized Computational Fluid Dynamics Approach for Journal Bearing Performance Prediction," Proc. Inst. Mech. Eng., Part J, **209**(2), pp. 99–108.

[134] Shenoy, B. S., Pai, R. S., Rao, D. S., and Pai, R., 2009, "Elasto-Hydrodynamic Lubrication Analysis of Full 360° Journal Bearing Using CFD and FSI Techniques," World J. Model. Simul., **5**(4), pp. 315–320.

[135] Li, Q., Liu, S., Pan, X., and Zheng, S., 2012, "A New Method for Studying the 3D Transient Flow of Misaligned Journal Bearings in Flexible Rotor-Systems," J. Zhejiang Univ., Sci., A, **13**(4), pp. 293–310.

[136] Lin, Q., Wei, Z., Wang, N., and Chen, W., 2013, "Analysis on the Lubrication Performances of Journal Bearing System Using Computational Fluid Dynamics and Fluid-Structure Interaction Considering Thermal Influence and Cavitation," Tribol. Int., **64**, pp. 8–15.

[137] Song, Y., and Gu, C., 2015, "Development and Validation of a Three-Dimensional Computational Fluid Dynamics Analysis for Journal Bearings Considering Cavitation and Conjugate Heat Transfer," ASME J. Eng. Gas Turbines Power, **137**(12), p. 122502.

[138] Edney, L. E., Heitland, G. B., and Decalmillo, S. M., 1998, "Testing, Analysis, and CFD Modeling of a Profiled Leading Edge Groove Tilting Pad Journal Bearing," 1998 ASME TURBO EXPO Conference, Stockholm, Sweden, June 2–5, ASME Paper No. 98-GT-409.

[139] Armentrout, R. W., He, M., Haykin, T., and Reed, A., 2017, "Analysis of Turbulence and Convective Inertia in a Water-Lubricated Tilting-Lubricated Tilting-Pad Journal Bearing Using Conventional and CFD Approaches," Tribol. Trans., **60**(6), pp. 1129–1147.

[140] Hagemann, T., and Schwarze, H., 2019, "Theoretical and Experimental Analyses of Directly Lubricated Tilting-Pad Journal Bearings With Leading Edge Groove," ASME J. Eng. Gas Turbines Power, **141**(5), p. 051010.

[141] Ding, A., Ren, X., Li, X., and Gu, C., 2018, "Friction Power Analysis and Improvement for a Tilting-Pad Journal Bearing Considering Air Entrainment," Appl. Therm. Eng., **145**(25), pp. 763–771.

[142] Li, M., Gu, C., Pan, X., Zheng, S., and Li, Q., 2016, "A New Dynamic Mesh Algorithm for Studying the 3D Transient Flow Field of Tilting Pad Journal Bearings," Proc. Inst. Mech. Eng., Part J, **230**(12), pp. 1470–1482.

[143] Liu, H., Xu, H., Ellison, P. J., and Jin, Z., 2010, "Application of Computational Fluid Dynamics and Fluid-Structure Interaction Method to the Lubrication Study of a Rotor-Bearing System," Tribol. Lett., **38**, pp. 324–336.

[144] Concli, F., 2016, "Pressure Distribution in Small Hydrodynamic Journal Bearings Considering Cavitation: a Numerical Approach Based on the Opensource CFD Code OpenFOAM®," Lubr. Sci., **28**(6), pp. 329–347.

[145] Crone, P., Almqvist, A., and Larsson, R., 2018, "Thermal Turbulent Flow in Leading Edge Grooved and Conventional Tilting Pad Journal Bearing Segments—A Comparative Study," Lubricants, **6**(4), p. 97.

[146] Maneshian, B., and Gandjalikhan Nassab, S. A., 2009, "Thermohydrodynamic Characteristics of Journal Bearings Running Under Turbulent Condition," Int. J. Eng., Trans. A, **22**(2), pp. 181–194.

[147] Montazeri, H., 2008, "Numerical Analysis of Hydrodynamic Journal Bearings Lubricated With Ferrofluid," Proc. Inst. Mech. Eng., Part J, **222**(1), pp. 51–60.

[148] Gertzos, K. P., Nikolakopoulos, P. G., and Papadopoulos, C. A., 2008, "CFD Analysis of Journal Bearing Hydrodynamic Lubrication by Bingham Lubricant," Tribol. Int., **41**(12), pp. 1190–1204.

[149] Gao, G., Yin, Z., Jiang, D., and Zhang, X., 2013, "CFD Analysis of Load-Carrying Capacity of Hydrodynamic Lubrication on a Water-Lubricated Journal Bearing," Ind. Lubr. Tribol., **67**(1), pp. 30–37.

[150] Gao, G., Yin, Z., Jiang, D., and Zhang, X., 2014, "Numerical Analysis of Plain Journal Bearing Under Hydrodynamic Lubrication by Water," Tribol. Int., **75**, pp. 31–38.

[151] Gao, G., Yin, Z., Jiang, D., Zhang, X., and Wang, Y., 2015, "Analysis on Design Parameters of Water-Lubricated Journal Bearings Under Hydrodynamic Lubrication," Proc. Inst. Mech. Eng., Part J, **230**(8), pp. 1019–1029.

[152] Wang, Y., Yin, Z., Jiang, D., Gao, G., and Zhang, X., 2015, "Study of the Lubrication Performance of Water-Lubricated Journal Bearings With CFD and FSI Method," Ind. Lubr. Tribol., **68**(3), pp. 341–348.

[153] Zhang, X., Yinn, Z., Jiang, D., Gao, G., Wang, Y., and Wang, X., 2016, "Load Carrying Capacity of Misaligned Hydrodynamic Water-Lubricated Plain Journal Bearings With Rigid Bush Materials," Tribol. Int., **99**, pp. 1–13.

[154] Arghir, M., Roucou, N., Helene, M., and Frene, J., 2003, "Theoretical Analysis of the Incompressible Laminar Flow in a Macro-Roughness Cell," ASME J. Tribol., **125**(2), pp. 309–318.

[155] Brajdic-Mitidieri, P., Gosman, A. D., Ioannides, E., and Spikes, H. A., 2005, "CFD Analysis of a Low Friction Pocketed Pad Bearing," ASME J. Tribol., **127**(4), pp. 803–812.

[156] Sahlin, F., Glavatskih, S. B., Almqvist, T., and Larsson, R., 2005, "Two-Dimensional CFD-Analysis of Micro-Patterned Surfaces in Hydrodynamic Lubrication," ASME J. Tribol., **127**(1), pp. 96–102.

[157] Han, J., Fang, L., Sun, J., and Ge, S., 2010, "Hydrodynamic Lubrication of Microdimple Textured Surface Using Three-Dimensional CFD," Tribol. Trans., **53**(6), pp. 860–870.

[158] Liang, X., Liu, Z., Wang, H., Zhou, X., and Zhou, X., 2016, "Hydrodynamic Lubrication of Partial Textured Sliding Journal Bearing Based on Three-Dimensional CFD," Ind. Lubr. Tribol., **68**(1), pp. 106–115.

[159] Fu, G., and Untaroiu, A., 2017, "A Study of the Effect of Various Recess Shapes on Hybrid Journal Bearing Performance Using Computational Fluid Dynamics and Response Surface Method," ASME J. Tribol., **139**(6), p. 061104.

[160] Yang, J., and Palazzolo, A., 2020, "Computational Fluid Dynamics Based Mixing Prediction for Tilt Pad Journal Bearing TEHD Modeling—Part I: TEHD-CFD Model Validation and Improvements," ASME J. Tribol., **143**(1), p. 011801.

[161] Yang, J., and Palazzolo, A., 2020, "Computational Fluid Dynamics Based Mixing Prediction for Tilt Pad Journal Bearing TEHD Modeling—Part II: Implementation With Machine Learning," ASME J. Tribol., **143**(1), p. 011802.